

Enriching continuous Lagrange finite element approximation spaces using neural networks

Hélène Barucq², Michel Duprez¹, Florian Faucher², Emmanuel Franck³, Frédérique Lecourtier^{*1}, Vanessa Lleras^{1,4}, Victor Michel-Dansac³, and Nicolas Victorion²

¹Project-Team MIMESIS, Inria, University of Strasbourg, ICube, CNRS UMR 7357, Strasbourg, France

²Project-Team Makutu, Inria, University of Pau and Pays de l'Adour, TotalEnergies, CNRS UMR 5142, Pau, France

³Project-Team MACARON, Inria, University of Strasbourg, IRMA, CNRS UMR 7501, Strasbourg, France

⁴IMAG, University of Montpellier, CNRS UMR 5149, Montpellier, France

February 10, 2025

Abstract

In this work, we present a preliminary study combining two approaches in the context of solving PDEs: the classical finite element method (FEM) and more recent techniques based on neural networks. Indeed, in recent years, physics-informed neural networks (PINNs) have become particularly interesting for rapidly solving such problems, especially in high dimensions. However, their lack of accuracy is a significant drawback in this context, hence the interest in combining them with FEM, for which error estimators are already known. The complete pipeline proposed here, therefore, consists of modifying classical FEM approximation spaces by taking information from a prior, chosen here as the prediction of a neural network. On the one hand, this combination improves and certifies the prediction of neural networks to obtain a fast and accurate solution. On the other hand, error estimates are proven, showing that such strategies outperform classical ones by a factor that depends only on the quality of the prior. We validate our approach with numerical results obtained for this preliminary work on parametric problems with one- and two-dimensional geometries. They demonstrate that to achieve a fixed error target, a coarser mesh can be used with our enhanced FEM compared to the standard one, leading to reduced computation time, particularly for parametric problems.

Contents

1	Introduction	3
2	Continuous finite element method	4
3	Enriching the finite element method with additive priors	6
3.1	Construction of the modified problem	6
3.2	Convergence analysis	6
4	Enriching the finite element method with multiplicative priors	8
4.1	Construction of the modified problem	8
4.2	Convergence analysis	9

*Corresponding author

5	Comparison of the two enriched methods	10
6	Prior construction using parametric PINNs	13
6.1	Physics-Informed Neural Networks for parametric PDEs	13
6.2	Improving PINN training and prediction	15
6.2.1	Exact imposition of boundary conditions	15
6.2.2	Sobolev training for PINNs	16
6.2.3	Overcoming the spectral bias	16
7	Implementation details	16
7.1	Using PINN prediction effectively	17
7.2	Imposing boundary conditions	17
7.2.1	Additive approach	17
7.2.2	Multiplicative approach	18
8	Numerical results	18
8.1	Setup of the numerical experiments	19
8.1.1	Error estimates	19
8.1.2	Gains achieved with the enriched bases	19
8.2	1D Poisson problem	20
8.2.1	Construction of the two priors	21
8.2.2	Error estimates — with the PINN prior	22
8.2.3	Derivatives — with both priors	23
8.2.4	Gains achieved with the additive and multiplicative approaches – with both priors	24
8.3	1D general elliptic system and convection-dominated regime	25
8.3.1	Error estimates	26
8.3.2	Comparison of different approaches	27
8.3.3	Gains achieved with the additive and the multiplicative approaches	28
8.4	2D Poisson problem in a square domain	29
8.4.1	Low-frequency case	29
8.4.1.1	Error estimates	30
8.4.1.2	Comparison of different approaches	31
8.4.1.3	Gains achieved with the additive approach	32
8.4.1.4	Costs of the different methods	33
8.4.1.5	Integration of analytical functions	34
8.4.2	Low-frequency case — Sobolev training	35
8.4.2.1	Error estimates	35
8.4.2.2	Gains achieved with the additive approach	36
8.4.3	Low-frequency case — Boundary loss training	36
8.4.3.1	Error estimates	37
8.4.3.2	Gains achieved with the additive approach	37
8.4.4	High-frequency case	38
8.4.4.1	Error estimates	38
8.4.4.2	Comparison of different approaches	39
8.4.4.3	Gains achieved with the additive approach	40
8.5	2D anisotropic elliptic problem on a square	41
8.5.1	Error estimates	42
8.5.2	Comparison of different approaches	42
8.5.3	Gains achieved with the additive approach	43
8.6	2D Poisson problem on an annulus, with mixed boundary conditions	44
8.6.1	Error estimates	45
8.6.2	Comparison of different approaches	46
8.6.3	Gains achieved with the additive approach	46

9 Conclusion and future works	47
10 Acknowledgment	47
A Notations and definitions	51

1 Introduction

The finite element method (FEM, e.g., [Cia02, EG04, BS08]) is a widely used method for the numerical solution of PDEs. It requires the construction of the mesh that discretizes the domain of interest into elements, typically simplexes or quadrilaterals/hexahedrals. Basis functions are associated to each element to define the approximation space in which the numerical solution is sought. This solution is defined from degrees of freedom, which depend on the elements and basis functions, and by the order of approximation of the method. In particular, the method converges according to the characteristic mesh size and, depending on the mesh size, it requires the inversion of a potentially large matrix. Hence, solving the problem thousands of times (as in optimal control or uncertainty propagation) becomes expensive. This has motivated intensive research on new finite element methods to combine accuracy and matrices of reduced orders. We can, for instance, refer to the Trefftz method (e.g., [HMP13, MP18, IGMS22]), or the hybridizable discontinuous Galerkin method (e.g., [CDG08, HPS17, PFB24]) where the resulting matrix uses degrees of freedom only on the skeleton of the mesh. In addition to the computational cost, it is important to note that one needs a mesh of the discretized geometry to perform the computation. This step is not always straightforward (e.g., in geosciences where Earth layers are not clearly localized), and it can be time-consuming. That is why mesh-less strategies have also been investigated in the last decades, and isogeometric analysis has been employed, e.g. [HCB05, FBCD22].

In recent years, learning-based alternatives have emerged, such as Physics-Informed Neural Networks (PINNs, [RPK19]) or the Deep Ritz method [EY18]. The idea is to approximate the solution of the PDE under consideration using a neural network trained by minimizing a loss function, taking the underlying physics into account. Unlike neural networks trained with more conventional data-driven loss functions, these methods share similarities with traditional solvers: They require the same inputs, namely the PDE, physical parameters, boundary, and initial conditions. In addition, the training phase requires approximating the PDE solution in a discrete set of points of the space domain. Thus, these approaches have some advantages, notably the absence of meshing and their relative dimension-insensitivity. Since they do not require data (reference solutions), they are particularly well suited to high-dimensional problems on complex domains. However, at present, these learning-based techniques are not competitive with classical finite element methods (see [GKLS24]), mainly because network-based methods lack precision and convergence guarantees, see [SKPP24] for a comparison between PINNs and FEM. While FEM has a better error/computation time ratio for a single resolution, PINNs are more advantageous for parametric systems where a multitude of resolutions is needed. We further refer to [CDCG+22] for some analysis on PINNs.

This paper aims to propose a new method that combines learning-based and finite element methods. More precisely, the main idea is to use a parametric PINN to compute a large family of offline solutions. This is followed by calculating an online solution for a single parameter using coarse finite elements, with the PINN solution used as a prior information. The result is a method capable of rapidly predicting a PDE solution while guaranteeing convergence properties, thanks to the FEM framework. Finite element resolution improves the prediction while remaining cheap as it is performed on a coarse mesh, benefiting from the network prediction. This paper proposes two ways to enrich the FEM. In both cases, the finite element error will be exhibited as a function of the network error with respect to the true solution. These corrections will be called “additive” and “multiplicative” depending on how the prediction is incorporated in the FEM spaces.

Some previous works combine FEM and the use of a prior as neural network prediction. In [BMP+19], the authors initialize Newton’s algorithm when solving a hyperelastic equation with a prior derived from the prediction of a neural network. Such a prediction can also be used as a prior for discontinuous Galerkin methods (see [FMDN24]). In [FST+24], the authors solve PDE by using a neural network for the spatial resolution and a FEM scheme for the temporal one. It is also possible to include the shape function of the FEM in a PINN approach as in [SDSG24]. In the φ -FEM method developed in [DL20] (see also [CDL+23, DLL22, DLLV23, DLL23] for

different contexts), the a priori of the FEM is a level set function used to localized the boundary of the domain. In the FEM, the space of approximation can also be enrich to ensure stability as for instance the introduction of bubble function in mixed problems (see e.g. [EG04]).

In this paper, we consider general parametric linear elliptic differential equations defined on a smooth domain $\Omega \subset \mathbb{R}^d$ with d space dimensions and $\partial\Omega$ the boundary of Ω . Let a parameter space $\mathcal{M} = \{\boldsymbol{\mu} = (\mu_1, \dots, \mu_p) \in \mathbb{R}^p\}$. The typical problem of interest is given by: for one or several $\boldsymbol{\mu} \in \mathcal{M}$, find $u : \Omega \rightarrow \mathbb{R}$ such that

$$\mathcal{L}(u; \boldsymbol{x}, \boldsymbol{\mu}) = f(\boldsymbol{x}, \boldsymbol{\mu}), \quad (1.1)$$

with $\boldsymbol{x} = (x_1, \dots, x_d) \in \Omega$ the space variable and where \mathcal{L} is the parametric differential operator defined by

$$\mathcal{L}(\cdot; \boldsymbol{x}, \boldsymbol{\mu}) : u \mapsto R(\boldsymbol{x}, \boldsymbol{\mu})u + C(\boldsymbol{\mu}) \cdot \nabla u - \frac{1}{\text{Pe}} \nabla \cdot (D(\boldsymbol{x}, \boldsymbol{\mu}) \nabla u),$$

with $f(\boldsymbol{x}, \boldsymbol{\mu}) \in L^2(\Omega)$ the source term, $R(\boldsymbol{x}, \boldsymbol{\mu}) \in L^\infty(\Omega)$ the reaction coefficient, $C(\boldsymbol{\mu}) \in \mathbb{R}^d$ the convection coefficient, $D(\boldsymbol{x}, \boldsymbol{\mu}) \in (W^{1,\infty}(\Omega))^{d \times d}$ the diffusion matrix (symmetric positive definite) and $\text{Pe} \in \mathbb{R}_+^*$ the Péclet number represents the ratio between convection and diffusion. The differential operator is considered with Dirichlet, Neumann or Robin boundary conditions, which can also depend on $\boldsymbol{\mu}$.

The pipeline associated with our approaches is presented in Figure 1.

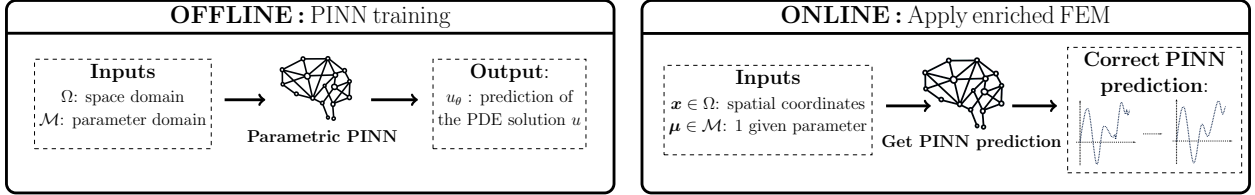


Figure 1: Pipeline of the enriched method considered. Left: offline phase (PINN training). Right: online phase (Correction of the PINN prediction).

The manuscript is organized as follows: In Section 2, we recall the used finite element method, allowing us to introduce the notations needed in the next sections. In Sections 3 and 4, we present the two proposed approaches and prove error estimates. They both rely on modifying the functions of the FEM approximation space, using information from prior knowledge of the solution. This prior is introduced first in an additive way, then in a multiplicative way. Both approaches are compared in Section 5. Section 6 is devoted to the construction of the prior, justifying the use of PINNs and recalling methods for improving their efficiency. In Section 7, we give details on the implementation. Numerical simulations conclude this manuscript in Section 8 and show that the proposed methods can significantly reduce the computational cost of solving parametric problems.

In Appendix A, we introduce the main notations used throughout this manuscript.

2 Continuous finite element method

The goal of this section is to recall the classical FEM, and to introduce the notation that will be used throughout the paper. To solve the problem (1.1) under consideration for a fixed parameter $\boldsymbol{\mu}$ (which will be omitted for clarity) with homogeneous Dirichlet boundary conditions using the continuous FEM, we rewrite it as the following variational problem:

$$\text{Find } u \in V^0 \text{ such that, } \forall v \in V^0, a(u, v) = l(v), \quad (2.1)$$

where $V^0 = H_0^1(\Omega)$, and where the bilinear form a is given by

$$a(u, v) = \frac{1}{\text{Pe}} \int_{\Omega} D \nabla u \cdot \nabla v + \int_{\Omega} R u v + \int_{\Omega} v C \cdot \nabla u,$$

while the linear form l reads

$$l(v) = \int_{\Omega} f v.$$

Remark 1. Note that since a is continuous on $V^0 \times V^0$ and coercive and l is continuous on V^0 , the existence and uniqueness of the solution u are ensured by the Lax-Milgram theorem.

Let \mathcal{T}_h be a mesh of the domain Ω composed of simplexes, where h denotes the characteristic size of the mesh, i.e. the biggest diameter of the simplexes. We suppose that \mathcal{T}_h satisfies the Ciarlet condition (see e.g. [EG04]) and that its boundary is exactly $\partial\Omega$. Consider $V_h^0 \subset V_h \subset V = H^1(\Omega)$ the two continuous Lagrange finite elements spaces of degree $k \geq 1$ defined by

$$V_h = \{v_h \in C^0(\Omega), \forall K \in \mathcal{T}_h, v_h|_K \in \mathbb{P}_k\}, \quad (2.2)$$

and

$$V_h^0 = \{v_h \in C^0(\Omega), \forall K \in \mathcal{T}_h, v_h|_K \in \mathbb{P}_k, v_h|_{\partial\Omega} = 0\},$$

with \mathbb{P}_k the space of polynomials with real coefficients of degree at most k . The solution to (2.1) will be approximated by the solution u_h to

$$\text{Find } u_h \in V_h^0 \text{ such that, } \forall v_h \in V_h^0, a(u_h, v_h) = l(v_h). \quad (2.3)$$

Let us now some results used in the next sections. We first introduce the Lagrange interpolation operator defined by

$$\mathcal{I}_h : C^0(\Omega) \ni v \mapsto \sum_{i=1}^{N_{\text{dofs}}} v(\mathbf{x}^{(i)})\psi_i \in V_h, \quad (2.4)$$

with $(\mathbf{x}^{(i)})_{i \in \{1, \dots, N_{\text{dofs}}\}}$ the N_{dofs} degrees of freedom (dofs) associated to the mesh, and $(\psi_i)_{i \in \{1, \dots, N_{\text{dofs}}\}}$ the associated Lagrange shape functions of degree k .

Remark 2. In the whole manuscript, for a Sobolev space H , the notation $|\cdot|_H$ and $\|\cdot\|_H$ will represent respectively the semi-norm and the norm in H .

The following result gives a bound of the interpolation error:

Theorem 3 (see e.g. [EG04]). *There exists $C_q > 0$ such that for all $v \in H^{q+1}(\Omega)$ and $1 \leq q \leq k$,*

$$\|v - \mathcal{I}_h v\|_{H^1} \leq C_q h^q |v|_{H^{q+1}}.$$

The next estimate is associated to the elliptic regularity:

Theorem 4 (see e.g. [Eva22, Theorem 4, p. 317]). *There exists $C_e > 0$, such that for all $f \in L^2(\Omega)$, the unique solution $w \in H^2(\Omega)$ to*

$$\mathcal{L}^* w = \xi$$

with homogeneous Dirichlet boundary condition satisfies

$$\|w\|_{H^2} \leq C_e \|\xi\|_{L^2}.$$

Here \mathcal{L}^* represents the adjoint of the operator \mathcal{L} .

These estimates, combined with Céa's Lemma, which uses the continuity and coercivity of a , give the following error estimate:

Theorem 5 (see e.g. [EG04]). *Let $u \in H^{q+1}(\Omega)$ and $u_h \in V_h^0$ the solutions to (2.1) and (2.3). For all $1 \leq q \leq k$, one has*

$$|u - u_h|_{H^1} \leq C_q \frac{\gamma}{\alpha} h^q |u|_{H^{q+1}}$$

and

$$\|u - u_h\|_{L^2} \leq C_e C_1 C_q \frac{\gamma^2}{\alpha} h^{q+1} |u|_{H^{q+1}},$$

where γ and α are respectively the constants of continuity and coercivity of a .

For the sake of simplicity, we consider an elliptic boundary value problem with homogeneous Dirichlet conditions. Obviously, we can use more general boundary conditions as Robin-like conditions depending on the parameters. This will be investigated in the numerical experiments to show that the proposed methodology applies to a larger class of boundary value problems, see Section 8.6.

3 Enriching the finite element method with additive priors

In this section, we assume that a prior knowledge of the solution to (1.1) is available. In what follows, we call this information a “prior”. This prior is denoted by $\mathbf{x} \mapsto u_\theta(\mathbf{x})$ with parameters θ , and we assume that it can be constructed with the desired regularity $u_\theta \in H^{q+1}(\Omega) \cap H_0^1(\Omega)$ for $1 \leq q \leq k$, where k is the polynomial degree of the enriched FEM. In this section and the next two, the prior will be general, but up the Section 6, it will be the prediction of a parametric PINN. In Section 3.1, we first show how to use this prior to enriching classical finite element spaces. Then, in Section 3.2, we prove a convergence estimate for the resulting method.

3.1 Construction of the modified problem

In the general setting of FEM, we follow the Bobunov–Galerkin method [EG04], where the basis functions and the numerical solutions are in the same space (see (2.3), where both u_h and v_h are in V_h^0). As we intend to enrich the classical approximation space, we exploit the idea formalized as Petrov–Galerkin method (e.g., [Red19, BS08, Dem23]), where the test and trial functions belong to different spaces. This approach is often used for convection-dominated problems, [AS97]. We propose to enrich the trial space using the prior u_θ such that,

$$V_h^+ = \{u_h^+ = u_\theta + p_h^+, \quad p_h^+ \in V_h^0\}, \quad (3.1)$$

and we use the space V_h^0 for the test functions. Since we have assumed that $u_\theta \in H^{q+1}(\Omega) \cap H_0^1(\Omega)$, V_h^+ is also a subset of V^0 , like V_h^0 . Plugging this new trial space into the approximate problem (2.3), we obtain the formulation

$$\text{Find } u_h^+ \in V_h^+ \text{ such that, } \forall v_h \in V_h^0, \quad a(u_h, v_h) = l(v_h), \quad (3.2)$$

which leads to the following approximation problem:

$$\text{Find } p_h^+ \in V_h^0 \text{ such that, } \forall v_h \in V_h^0, \quad a(p_h^+, v_h) = l(v_h) - a(u_\theta, v_h). \quad (3.3)$$

Therefore, we obtain a classical Galerkin approximation with a modified source term.

3.2 Convergence analysis

The objective is to prove that the FEM solution to problem (3.3) converges, with an error depending on the quality of the prior.

Theorem 6. *Let $u \in H^{q+1}(\Omega)$ be the solution to problem (2.1) and $u_\theta \in H^{q+1}(\Omega) \cap H_0^1(\Omega)$ be a prior on u . We consider $u_h^+ \in V_h^+$ as the solution to the discrete problem (3.3) with V_h^+ the modified trial space defined in (3.1). The following estimates hold. For all $1 \leq q \leq k$,*

$$|u - u_h^+|_{H^1} \leq C_q \frac{\gamma}{\alpha} C_{\text{gain}}^+ h^q |u|_{H^{q+1}} \quad (3.4)$$

and

$$\|u - u_h^+\|_{L^2} \leq C_e C_1 C_q \frac{\gamma^2}{\alpha} C_{\text{gain}}^+ h^{q+1} |u|_{H^{q+1}},$$

with $C_e, C_1, C_q, \gamma, \alpha$ defined in Section 2 and

$$C_{\text{gain}}^+ = \frac{|u - u_\theta|_{H^{q+1}}}{|u|_{H^{q+1}}}. \quad (3.5)$$

Remark 7. *The constant C_{gain}^+ represents the potential gain compared to the error of the classical FEM presented in Theorem 5. Note that this constant is the same in L^2 norm and H^1 semi-norm.*

Proof of Theorem 6. H^1 -error: To prove (3.4), we adapt the proof of Céa’s lemma to the additive prior case. Considering the trial space defined in (3.1), the numerical solution u_h^+ is given by

$$u_h^+ = u_\theta + p_h^+,$$

with $p_h^+ \in V_h^0 \subset V$ solution to (3.3). We have

$$\begin{aligned} a(u - u_h^+, u - u_h^+) &= a(u - u_h^+, (u - u_\theta) - p_h^+ - v_h + v_h), & \forall v_h \in V_h^0 \\ &= a(u - u_h^+, (u - u_\theta) - v_h) + a(u - u_h^+, v_h - p_h^+), & \forall v_h \in V_h^0. \end{aligned} \quad (3.6)$$

Let us first estimate the second term on the right-hand side of (3.6). Using the fact that $V_h^0 \subset V^0$, we have, by Galerkin orthogonality (difference of the continuous problem (2.1) and discrete problem (3.2)),

$$a(u - u_h^+, z_h) = 0, \quad \forall z_h \in V_h^0. \quad (3.7)$$

Therefore, for $z_h = v_h - p_h^+ \in V_h^0$, we obtain

$$a(u - u_h^+, v_h - p_h^+) = 0, \quad \forall v_h \in V_h^0.$$

Plugging this equality into (3.6) yields

$$a(u - u_h^+, u - u_h^+) = a(u - u_h^+, (u - u_\theta) - v_h), \quad \forall v_h \in V_h^0.$$

Denoting by α and γ the coercivity and continuity constants of the bilinear form a , we have

$$\begin{aligned} \alpha |u - u_h^+|_{H^1}^2 &\leq a(u - u_h^+, u - u_h^+) = a(u - u_h^+, (u - u_\theta) - v_h), & \forall v_h \in V_h^0, \\ &\leq \gamma |u - u_h^+|_{H^1} |(u - u_\theta) - v_h|_{H^1}, & \forall v_h \in V_h^0, \end{aligned}$$

which immediately leads to

$$|u - u_h^+|_{H^1} \leq \frac{\gamma}{\alpha} |(u - u_\theta) - v_h|_{H^1}, \quad \forall v_h \in V_h^0.$$

Since the above relation is valid for all $v_h \in V_h^0$, we apply it to $v_h = \mathcal{I}_h(u - u_\theta) \in V_h^0$ with \mathcal{I}_h the Lagrange interpolation operator (2.4) in V_h , it holds using interpolation estimate given in Theorem 3,

$$|u - u_h^+|_{H^1} \leq C_q \frac{\gamma}{\alpha} h^q |u - u_\theta|_{H^{q+1}},$$

with C_q defined in Section 2.

The above expression can be rewritten as

$$|u - u_h^+|_{H^1} \leq C_q \frac{\gamma}{\alpha} C_{\text{gain}}^+ h^q |u|_{H^{q+1}}, \quad (3.8)$$

with

$$C_{\text{gain}}^+ = \frac{|u - u_\theta|_{H^{q+1}}}{|u|_{H^{q+1}}},$$

which completes the first part of the proof.

L^2 -error: We will follow the Aubin-Nitsche technique. Consider $w \in H^2(\Omega)$ the solution to

$$\mathcal{L}^* w = u - u_h^+,$$

with homogeneous Dirichlet boundary condition. Thanks to Theorem 4, one has

$$\|w\|_{H^2} \leq C_e \|u - u_h^+\|_{L^2}. \quad (3.9)$$

Using the Galerkin orthogonality (3.7) and the continuity of the bilinear form a ,

$$\|u - u_h^+\|_{L^2}^2 = a(u - u_h^+, w - I_h w) \leq \gamma |u - u_h^+|_{H^1} |w - I_h w|_{H^1}.$$

Thanks to Theorem 3 and (3.9),

$$|w - I_h w|_{H^1} \leq C_e C_1 \|u - u_h^+\|_{L^2},$$

which leads to the conclusion by using (3.8). \square

Remark 8. The gain constant C_{gain}^+ defined in (3.5) shows that the closer the prior is to the solution, the smaller is the error constant associated with the FEM while keeping the same order of accuracy. Therefore, as soon as $C_{\text{gain}}^+ < 1$, the FEM with additive prior will be more accurate than the classical one. While this gives us a particularly flexible constraint, our objective is to balance this gain by relaxing the contribution h^q , using a coarser grid and low-order polynomial, to reduce the computational cost of the FEM while maintaining accuracy. Nonetheless, the gain is related to the L^2 error associated with the derivatives of $(q+1)^{\text{th}}$ order (with $1 \leq q \leq k$) of the prior. This shows that the prior must accurately approximate the derivatives of the solution in addition to the solution itself. This highlights that we need to build our prior by ensuring a good approximation of the derivatives of the solution. It also shows that the higher the order of the finite elements k is, the better our prior should approximate the higher-order derivatives. Therefore, it is more appropriate to use only low-order FEM so that k remains small.

4 Enriching the finite element method with multiplicative priors

This section employs the same assumptions as in Section 3, namely that we have a sufficiently smooth prior u_θ on the solution u of the PDE (1.1). However, this prior will now be multiplied to elements of V_h rather than added to them. We construct the underlying modified problem in Section 4.1. Then, similarly to the additive approach of Section 3, error estimates are obtained in Section 4.2.

4.1 Construction of the modified problem

To construct the modified problem in this case, we must ensure that the prior u_θ never vanishes. Therefore, we propose to modify the initial problem (1.1) and consider in this section the problem defined by

$$\begin{cases} \mathcal{L}(u_M) = f, & \text{in } \Omega, \\ u_M = M, & \text{on } \partial\Omega. \end{cases} \quad (4.1)$$

Note that (4.1) is nothing but the initial problem (1.1) lifted by a constant $M \in \mathbb{R}_+$, chosen large enough to ensure that $u_M = u + M > 0$. We then introduce the associated variational problem, defined by

$$\text{Find } u_M = u + M, \text{ with } u \in V^0 \text{ such that, } \forall v \in V^0, a(u_M, v) = l(v). \quad (4.2)$$

Therefore, solving (4.2), we recover the solution u of the initial problem (1.1) by setting

$$u = u_M - M.$$

The prior

$$u_{\theta, M} = u_\theta + M > 0$$

is associated with problem (4.2).

Let us introduce the following modified finite element space defined by

$$V_h^\times = \left\{ u_{h, M}^\times = u_{\theta, M} p_h^\times, \quad p_h^\times \in 1 + V_h^0 \right\}, \quad (4.3)$$

with, for all $\mathbf{x} \in \Omega$, $u_{\theta, M}(\mathbf{x}) \neq 0$. From (4.2), this leads to the following approximate formulation:

$$\text{Find } p_h^\times \in 1 + V_h^0 \text{ such that, } \forall v_h \in V_h^0, \quad a(u_{\theta, M} p_h^\times, u_{\theta, M} v_h) = l(u_{\theta, M} v_h). \quad (4.4)$$

Therefore, solving (4.4), we recover the solution $u_h^\times \in V_h^\times - M$ of the original problem (1.1) by setting $u_h^\times = u_{h, M}^\times - M$.

Based on the N_{dofs} dofs $(\mathbf{x}^{(i)})_{i \in \{1, \dots, N_{\text{dofs}}\}}$ of the mesh, we consider the interpolation operator on V_h^\times given by

$$\tilde{\mathcal{I}}_h : C^0(\Omega) \ni v \mapsto \sum_{i=1}^{N_{\text{dofs}}} \frac{v(\mathbf{x}^{(i)})}{u_{\theta, M}(\mathbf{x}^{(i)})} \tilde{\psi}_i \in V_h^\times,$$

where the shape functions $\tilde{\psi}_i$ associated to V_h^\times are defined by

$$\tilde{\psi}_i = u_{\theta,M} \psi_i,$$

with ψ_i the classical shape functions presented in [Section 2](#). Note that the new interpolation operator $\tilde{\mathcal{I}}_h$ is related to the classical Lagrange interpolation operator defined in [\(2.4\)](#) as follows

$$\forall v \in C^0(\Omega), \quad \tilde{\mathcal{I}}_h(v) = u_{\theta,M} \mathcal{I}_h \left(\frac{v}{u_{\theta,M}} \right). \quad (4.5)$$

4.2 Convergence analysis

In this section, we finally prove that the modified FEM [\(4.4\)](#) converges to the solution to [\(4.1\)](#), and that it satisfies the same type of estimate as the classical one. Equipped with the lifting trick in [Section 4.1](#), we can state the following convergence theorem.

Theorem 9. *Let $u_M \in H^{q+1}(\Omega)$ be the solution of the enhanced problem [\(4.2\)](#) and $u_{\theta,M} \in M + H^{q+1}(\Omega) \cap H_0^1(\Omega)$ be a priori on u_M . We consider $u_{h,M}^\times \in V_h^\times$ the solution to the finite element problem [\(4.4\)](#) with V_h^\times the modified trial space defined in [\(4.3\)](#), considering \mathbb{P}_k polynomials. We define $u = u_M - M$ and $u_h^\times = u_{h,M}^\times - M$. Then, for all $1 \leq q \leq k$*

$$|u - u_h^\times|_{H^1} \leq C_q \frac{\gamma}{\alpha} C_{\text{gain},H^1}^{\times,M} h^q |u|_{H^{q+1}}$$

and

$$\|u - u_h^\times\|_{L^2} \leq C_e C_1 C_q \frac{\gamma^2}{\alpha} C_{\text{gain},L^2}^{\times,M} h^{q+1} |u|_{H^{q+1}},$$

with $C_e, C_1, C_q, \gamma, \alpha$ defined in [Section 2](#), and where

$$C_{\text{gain},H^1}^{\times,M} = \left| \frac{u_M}{u_{\theta,M}} \right|_{H^{q+1}} \frac{\|u_{\theta,M}\|_{W^{1,\infty}}}{|u|_{H^{q+1}}}, \quad (4.6)$$

and

$$C_{\text{gain},L^2}^{\times,M} = C_{\theta,M} \left| \frac{u_M}{u_{\theta,M}} \right|_{H^{q+1}} \frac{\|u_{\theta,M}\|_{W^{1,\infty}}^2}{|u|_{H^{q+1}}}, \quad (4.7)$$

with

$$C_{\theta,M} = \|u_{\theta,M}^{-1}\|_{L^\infty} + 2|u_{\theta,M}^{-1}|_{W^{1,\infty}} + |u_{\theta,M}^{-1}|_{W^{2,\infty}}. \quad (4.8)$$

Remark 10. *The constants $C_{\text{gain},H^1}^{\times,M}$ and $C_{\text{gain},L^2}^{\times,M}$ represents the potential gains in both H^1 semi-norm and L^2 norm when using the multiplicative approach, compared to the error of the classical FEM presented in [Theorem 5](#) with \mathbb{P}_k polynomials.*

Proof of [Theorem 9](#). H^1 -error: Considering the trial space defined in [\(4.3\)](#), the numerical solution $u_{h,M}^\times$ is given by

$$u_{h,M}^\times = u_{\theta,M} p_h^\times,$$

with $p_h^\times \in 1 + V_h^0 \subset 1 + V^0$ solution to [\(4.4\)](#). By coercivity of a ,

$$\alpha |u_M - u_{h,M}^\times|_{H^1}^2 \leq a(u_M - u_{h,M}^\times, u_M - u_{h,M}^\times).$$

Thanks to [\(2.1\)](#) and [\(4.4\)](#), we have the following Galerkin orthogonality: for all $v_h \in V_h^0$,

$$a(u_M - u_{h,M}^\times, u_{\theta,M} v_h) = 0. \quad (4.9)$$

For $v_h = p_h^\times - \tilde{\mathcal{I}}_h \left(\frac{u_M}{u_{\theta,M}} \right)$, we deduce by definition [\(4.5\)](#) of $\tilde{\mathcal{I}}_h$ that

$$a(u_M - u_{h,M}^\times, u_M - u_{h,M}^\times) = a \left(u_M - u_{\theta,M} \tilde{\mathcal{I}}_h \left(\frac{u_M}{u_{\theta,M}} \right), u_M - u_{h,M}^\times \right) = a(u_M - \tilde{\mathcal{I}}_h(u_M), u_M - u_{h,M}^\times).$$

By continuity of a ,

$$|u_M - u_{h,M}^\times|_{H^1} \leq \frac{\gamma}{\alpha} |u_M - \tilde{\mathcal{I}}_h(u_M)|_{H^1}. \quad (4.10)$$

Again, using the definition (4.5) of $\tilde{\mathcal{I}}_h$,

$$|u_M - \tilde{\mathcal{I}}_h(u_M)|_{H^1} \leq \|u_{\theta,M}\|_{W^{1,\infty}} \left\| \frac{u_M}{u_{\theta,M}} - \mathcal{I}_h \left(\frac{u_M}{u_{\theta,M}} \right) \right\|_{H^1}.$$

Finally, applying interpolation estimate given in [Theorem 3](#), it holds

$$|u_M - \tilde{\mathcal{I}}_h(u_M)|_{H^1} \leq C_q \|u_{\theta,M}\|_{W^{1,\infty}} h^q \left| \frac{u_M}{u_{\theta,M}} \right|_{H^{q+1}}, \quad (4.11)$$

with C_q defined in [Section 2](#). Combining the last inequality with (4.10), we obtain

$$|u - u_h^\times|_{H^1} = |u_M - u_{h,M}^\times|_{H^1} \leq C_q \frac{\gamma}{\alpha} C_{\text{gain},H^1}^{\times,M} h^q |u|_{H^{q+1}}, \quad (4.12)$$

with $C_{\text{gain},H^1}^{\times,M}$ given in (4.6), which conclude the first part of the proof.

L^2 -error: Again, we follow the Aubin-Nitsche strategy here. Consider the problem

$$\mathcal{L}^* w = u - u_h^\times = u_M - p_h^\times u_{\theta,M},$$

with $w = M$ on $\partial\Omega$. Then, using the Galerkin orthogonality (4.9) for $v_h = \mathcal{I}_h \left(\frac{u_M}{u_{\theta,M}} \right)$,

$$\|u - u_h^\times\|_{L^2}^2 = \|u_M - p_h^\times u_{\theta,M}\|_{L^2}^2 = a(u_M - p_h^\times u_{\theta,M}, w) = a(u_M - p_h^\times u_{\theta,M}, w - \tilde{\mathcal{I}}_h(w)).$$

Hence, by continuity of a ,

$$\|u - u_h^\times\|_{L^2}^2 \leq \gamma |u_M - p_h^\times u_{\theta,M}|_{H^1} |w - \tilde{\mathcal{I}}_h(w)|_{H^1}.$$

Using (4.12) and (4.11) for $q = 1$ to the term in the right hand side,

$$\|u - u_h^\times\|_{L^2}^2 \leq C_1 C_q \frac{\gamma^2}{\alpha} \|u_{\theta,M}\|_{W^{1,\infty}} \left| \frac{w}{u_{\theta,M}} \right|_{H^2} C_{\text{gain},H^1}^{\times,M} h^{q+1} |u|_{H^{q+1}}.$$

Moreover

$$\left| \frac{w}{u_{\theta,M}} \right|_{H^2} \leq C_{\theta,M} \|w\|_{H^2},$$

with $C_{\theta,M}$ given in (4.8). Thanks to the elliptic regularity, we obtain

$$\|u - u_h^\times\|_{L^2} \leq C_e C_1 C_q \frac{\gamma^2}{\alpha} C_{\text{gain},L^2}^{\times,M} h^{q+1} |u|_{H^{q+1}},$$

with $C_{\text{gain},L^2}^{\times,M}$ defined in (4.7). □

Remark 11. We note that the gain constants $C_{\text{gain},H^1}^{\times,M}$ and $C_{\text{gain},L^2}^{\times,M}$ are similar to the constant C_{gain}^+ introduced in [Section 3](#), in that, it depends on high-order derivatives of the prior. Hence, a high-quality prior will necessarily involve a good approximation of the derivatives of the exact solution, and [Remark 8](#) also applies in the present context. The major difference with the additive approach lies in the choice of the lifting constant M . To better understand this dependency in M , the following section provides a study of the behaviour of our two gain constants when M goes to infinity. Moreover, the actual choice of M will be numerically investigated in [Section 8](#).

5 Comparison of the two enriched methods

This section aims to compare the two approaches proposed to improve the classical finite element method, the additive approach presented in [Section 3](#) and the multiplicative approach proposed in this [Section 4](#). Recall that the constant M is chosen in the multiplicative approach so that $u_M > 0$. Let u be the solution of problem (2.1) and $u_\theta \in H^{q+1}(\Omega) \cap H_0^1(\Omega)$ be a prior on u , with $1 \leq q \leq k$ (k the polynomial degree of the finite element method). Let us first recall the two approaches considered in the present paper:

Additive approach. We consider $u_h^+ \in V_h^+$ as the solution to the finite element method associated to problem (3.3) with V_h^+ the modified trial space defined in (3.1), considering \mathbb{P}_k polynomials. Using Theorem 6, we have for $1 \leq q \leq k$,

$$|u - u_h^+|_{H^1} \leq C_q \frac{\gamma}{\alpha} C_{\text{gain}}^+ h^q |u|_{H^{q+1}} \quad (5.1)$$

and

$$\|u - u_h^+\|_{L^2} \leq C_e C_1 C_q \frac{\gamma^2}{\alpha} C_{\text{gain}}^+ h^{q+1} |u|_{H^{q+1}}, \quad (5.2)$$

with $C_e, C_1, C_q, \gamma, \alpha$ defined in Section 2 and

$$C_{\text{gain}}^+ = \frac{|u - u_\theta|_{H^{q+1}}}{|u|_{H^{q+1}}}. \quad (5.3)$$

Multiplicative approach. Let $u_M = u + M$ be the solution of the enhanced problem (4.2) and $u_{\theta,M} = u_\theta + M$ be a prior on u_M . We consider $u_{h,M}^\times \in V_h^\times$ the solution to the finite element problem (4.4) with V_h^\times the modified trial space defined in (4.3), considering \mathbb{P}_k polynomials. We then recover the solution of the initial problem by taking $u_h^\times = u_{h,M}^\times - M$. Using Theorem 9, we have for $1 \leq q \leq k$,

$$|u - u_h^\times|_{H^1} \leq C_q \frac{\gamma}{\alpha} C_{\text{gain},H^1}^{\times,M} h^q |u|_{H^{q+1}} \quad (5.4)$$

and

$$\|u - u_h^\times\|_{L^2} \leq C_e C_1 C_q \frac{\gamma^2}{\alpha} C_{\text{gain},L^2}^{\times,M} h^{q+1} |u|_{H^{q+1}}, \quad (5.5)$$

with $C_e, C_1, C_q, \gamma, \alpha$ defined in Section 2, and

$$C_{\text{gain},H^1}^{\times,M} = \left| \frac{u_M}{u_{\theta,M}} \right|_{H^{q+1}} \frac{\|u_{\theta,M}\|_{W^{1,\infty}}}{|u|_{H^{q+1}}}, \quad (5.6)$$

and

$$C_{\text{gain},L^2}^{\times,M} = C_{\theta,M} \left| \frac{u_M}{u_{\theta,M}} \right|_{H^{q+1}} \frac{\|u_{\theta,M}\|_{W^{1,\infty}}^2}{|u|_{H^{q+1}}}, \quad (5.7)$$

with $C_{\theta,M}$ given in (4.8).

Comparison of the two approaches. The following result proves that the upper bound in (5.4) and in (5.5) converges to the one in (5.1) when M goes to infinity. In other words, the multiplicative gain constants defined in (5.6) and (5.7) converge to the additive gain constant defined in (5.3).

Theorem 12. *We have*

$$C_{\text{gain},H^1}^{\times,M} \xrightarrow{M \rightarrow \infty} C_{\text{gain}}^+ \quad (5.8)$$

and

$$C_{\text{gain},L^2}^{\times,M} \xrightarrow{M \rightarrow \infty} C_{\text{gain}}^+.$$

Proof. **Convergence in H^1 theoretical gain:** According to the expressions (5.3) and (5.6) of the gain constants, the objective of the proof is to show that

$$\|u_{\theta,M}\|_{W^{1,\infty}} \left| \frac{u_M}{u_{\theta,M}} \right|_{H^{q+1}} \xrightarrow{M \rightarrow \infty} |u - u_\theta|_{H^{q+1}}.$$

Denoting by

$$E_\theta = u - u_\theta,$$

the error made by the prior u_θ when approximating the solution u , we have

$$|u - u_\theta|_{H^{q+1}} = |E_\theta|_{H^{q+1}}.$$

On the one hand, we have that,

$$\|u_{\theta,M}\|_{W^{1,\infty}} = \|u_{\theta} + M\|_{W^{1,\infty}} = M \left\| 1 + \frac{u_{\theta}}{M} \right\|_{W^{1,\infty}}.$$

On the other hand, we have,

$$\left| \frac{u_M}{u_{\theta,M}} \right|_{H^{q+1}} = \left| \frac{u + M}{u_{\theta} + M} \right|_{H^{q+1}} = \left| \frac{u - u_{\theta} + u_{\theta} + M}{u_{\theta} + M} \right|_{H^{q+1}} = \left| 1 + \frac{u - u_{\theta}}{u_{\theta} + M} \right|_{H^{q+1}} = \frac{1}{M} \left| \frac{E_{\theta}}{1 + \frac{u_{\theta}}{M}} \right|_{H^{q+1}}.$$

Multiplying these expressions, we obtain

$$\|u_{\theta,M}\|_{W^{1,\infty}} \left| \frac{u_M}{u_{\theta,M}} \right|_{H^{q+1}} = \underbrace{\left\| 1 + \frac{u_{\theta}}{M} \right\|_{W^{1,\infty}}}_I \underbrace{\left| \frac{E_{\theta}}{1 + \frac{u_{\theta}}{M}} \right|_{H^{q+1}}}_{II}. \quad (5.9)$$

We now estimate term by term the right-hand side of the above equality (5.9), looking at their limits when M goes to infinity.

Term I: By decomposing the first term, we obtain

$$(I) = \left\| 1 + \frac{u_{\theta}}{M} \right\|_{W^{1,\infty}} = \left\| 1 + \frac{u_{\theta}}{M} \right\|_{L^{\infty}} + \frac{1}{M} \|\nabla u_{\theta}\|_{L^{\infty}} \xrightarrow{M \rightarrow \infty} 1,$$

since

$$1 - \frac{\|u_{\theta}\|_{\infty}}{M} \leq \left\| 1 + \frac{u_{\theta}}{M} \right\|_{L^{\infty}} \leq 1 + \frac{\|u_{\theta}\|_{\infty}}{M}. \quad (5.10)$$

Term II: Let us prove that

$$(II) = \left| \frac{E_{\theta}}{1 + \frac{u_{\theta}}{M}} \right|_{H^{q+1}} \xrightarrow{M \rightarrow \infty} |E_{\theta}|_{H^{q+1}}.$$

We have

$$\begin{aligned} \left| \left| \frac{E_{\theta}}{1 + \frac{u_{\theta}}{M}} \right|_{H^{q+1}}^2 - |E_{\theta}|_{H^{q+1}}^2 \right| &\leq \left| \frac{E_{\theta}}{1 + \frac{u_{\theta}}{M}} - E_{\theta} \right|_{H^{q+1}}^2 \\ &= \left\| \nabla^{q+1} \left(\frac{E_{\theta}}{1 + \frac{u_{\theta}}{M}} - E_{\theta} \right) \right\|_{L^2}^2 \leq |\Omega| \left\| \nabla^{q+1} \left(\frac{E_{\theta}}{1 + \frac{u_{\theta}}{M}} - E_{\theta} \right) \right\|_{L^{\infty}}^2. \end{aligned}$$

Then, using the general Leibniz rule, we have,

$$\begin{aligned} \left\| \nabla^{q+1} \left(\frac{E_{\theta}}{1 + \frac{u_{\theta}}{M}} - E_{\theta} \right) \right\|_{L^{\infty}} &\leq \left\| \frac{\nabla^{q+1} E_{\theta}}{1 + \frac{u_{\theta}}{M}} - \nabla^{q+1} E_{\theta} \right\|_{L^{\infty}} + \sum_{s=1}^{q+1} \binom{q+1}{s} \|\nabla^{q+1-s} E_{\theta}\|_{L^{\infty}} \left\| \nabla^s \left(\frac{1}{1 + \frac{u_{\theta}}{M}} \right) \right\|_{L^{\infty}} \\ &\leq \underbrace{\left\| \frac{\nabla^{q+1} E_{\theta}}{1 + \frac{u_{\theta}}{M}} - \nabla^{q+1} E_{\theta} \right\|_{L^{\infty}}}_{(1)} + \|E_{\theta}\|_{W^{q+1,\infty}} \sum_{s=1}^{q+1} \binom{q+1}{s} \underbrace{\left\| \nabla^s \left(\frac{1}{1 + \frac{u_{\theta}}{M}} \right) \right\|_{L^{\infty}}}_{(2)}. \end{aligned}$$

We now estimate terms (1) and (2) in the right-hand side of the above inequality.

Term (1): Taking $M > \|u_{\theta}\|_{L^{\infty}}$, we obtain

$$(1) \leq \left\| \frac{1}{1 + \frac{u_{\theta}}{M}} - 1 \right\|_{L^{\infty}} \|\nabla^{q+1} E_{\theta}\|_{L^{\infty}} \leq \frac{1}{M} \frac{\|u_{\theta}\|_{L^{\infty}}}{1 - \frac{\|u_{\theta}\|_{L^{\infty}}}{M}} \|\nabla^{q+1} E_{\theta}\|_{L^{\infty}} \xrightarrow{M \rightarrow \infty} 0.$$

Term (2): Using the Faà di Bruno formula and (5.10), there exists a constant $C > 0$ such that, for any $M > \|u_{\theta}\|_{L^{\infty}}$ and $1 \leq s \leq q+1$, the following estimate holds

$$(2) \leq C \frac{\prod_{m=0}^s \|\nabla^m \left(1 + \frac{u_{\theta}}{M} \right)\|_{L^{\infty}}}{\left\| 1 + \frac{u_{\theta}}{M} \right\|_{\infty}^{s+1}} \leq C \frac{1}{M^s} \frac{\left(1 + \frac{\|u_{\theta}\|_{\infty}}{M} \right) \prod_{m=1}^s \|\nabla^m u_{\theta}\|_{L^{\infty}}^s}{\left(1 - \frac{\|u_{\theta}\|_{\infty}}{M} \right)^{s+1}} \xrightarrow{M \rightarrow \infty} 0,$$

which leads to (5.8).

Convergence in L^2 theoretical gain: Using the convergence of the gain for the H^1 semi-norm, we only lead to prove that

$$C_{\theta,M} \|u_{\theta,M}\|_{W^{1,\infty}} \xrightarrow{M \rightarrow \infty} 1,$$

with $C_{\theta,M}$ given by

$$C_{\theta,M} = \|u_{\theta,M}^{-1}\|_{L^\infty} + 2|u_{\theta,M}^{-1}|_{W^{1,\infty}} + |u_{\theta,M}^{-1}|_{W^{2,\infty}}.$$

Since

$$\frac{1}{M} \|u_{\theta,M}\|_{W^{1,\infty}} \xrightarrow{M \rightarrow \infty} 1,$$

let us only prove that

$$MC_{\theta,M} \xrightarrow{M \rightarrow \infty} 1.$$

Considering $M > \|u_\theta\|_{L^\infty}$, we have

$$M \|u_{\theta,M}^{-1}\|_{L^\infty} = \left\| \frac{1}{1 + \frac{u_\theta}{M}} \right\|_{L^\infty} \leq \frac{1}{1 - \frac{\|u_\theta\|_{L^\infty}}{M}} \xrightarrow{M \rightarrow \infty} 1.$$

Moreover

$$2M |u_{\theta,M}^{-1}|_{W^{1,\infty}} = 2M \left\| \frac{\nabla u_\theta}{(u_\theta + M)^2} \right\|_{L^\infty} \xrightarrow{M \rightarrow \infty} 0.$$

Similarly

$$M |u_{\theta,M}^{-1}|_{W^{2,\infty}} \xrightarrow{M \rightarrow \infty} 0,$$

which leads to the conclusion. □

6 Prior construction using parametric PINNs

We have introduced new finite element approximation spaces in Sections 3 and 4 depending on the construction of priors. Physics-Informed Neural Networks (PINNs) are a good choice to build such priors. Indeed, since PINNs minimize the PDE residual, they inherently give a good approximation of the derivative of the solution, in addition to the solution itself (see e.g. [RPK19]). This section is therefore dedicated to introducing PINNs in Section 6.1, and then to show how to improve them in Section 6.2.

6.1 Physics-Informed Neural Networks for parametric PDEs

Physics-Informed Neural Networks, or PINNs, were introduced by [RPK19] for solving a PDE with Neural Networks. The main idea is to recast a PDE as an optimization problem. We illustrate the method on our problem (1.1), which we extend, in this section, to non-homogeneous Dirichlet boundary conditions. Moreover, we introduce a dependency on some physical parameters, making the problem of interest a parametric PDE. Unlike classical PINNs, which train for a specific case of boundary conditions or physical parameters, parametric PINNs seek to learn a generalized solution covering a range of parameters. They incorporate these parameters as additional inputs to the network, allowing greater flexibility in solving problems where physical conditions or properties vary. Moreover, since they are based on a combination of neural networks and the Monte-Carlo method, PINNs are ideally suited to solving such higher-dimensional problems.

Considering p parameters $\boldsymbol{\mu} = (\mu_1, \dots, \mu_p) \in \mathcal{M} \subset \mathbb{R}^p$, with some parameter space \mathcal{M} , the parametric PDE reads

$$\begin{cases} \mathcal{L}(u(\mathbf{x}, \boldsymbol{\mu}); \mathbf{x}, \boldsymbol{\mu}) = f(\mathbf{x}, \boldsymbol{\mu}), & \mathbf{x} \in \Omega, \\ u(\mathbf{x}, \boldsymbol{\mu}) = g(\mathbf{x}, \boldsymbol{\mu}), & \mathbf{x} \in \partial\Omega, \end{cases} \quad (6.1)$$

with g the trace of a H^2 function on $\partial\Omega$. Note that the solution of the equation depends on the parameters $\boldsymbol{\mu}$, as do the operator \mathcal{L} and the boundary conditions. This can be contrasted to the solution of (1.1), which only depended on the space variable \boldsymbol{x} . We then denote $u_\theta(\cdot, \boldsymbol{\mu})$ the approximate PINN prediction for given parameters $\boldsymbol{\mu}$.

The first idea of PINNs comes from the observation that, by construction, neural networks with smooth activation functions are nothing but smooth functions of their weights and inputs. Therefore, neural networks form natural candidates for approximating solutions to PDEs, especially with the advent of automatic differentiation tools. In our case, a PINN is a neural network that takes $d + p$ inputs, where d is the dimension of the space variable $\boldsymbol{x} \in \Omega$ and p is the number of parameters $\boldsymbol{\mu} \in \mathcal{M}$. We denote by $u_\theta(\boldsymbol{x}, \boldsymbol{\mu})$ the output, where θ are the learnable weights of the network. Classically, this neural network is a coordinate-based neural network, such as a multi-layer perceptron (MLP).

Remark 13. In Section 8, we need some notations describing how this PINN has been constructed. In particular, we will note σ the MLP activation function, and layers will describe an integer sequence describing the number of neurons associated with each layer of the MLP. For training, we will note lr for the learning rate and n_{epochs} the number of epochs considered, as well as decay the multiplicative factor of the learning rate decay considered every 20 epochs thanks to Pytorch's StepLR scheduler. Where this is not specified, the batch size will correspond to the number of collocation points chosen. The Adam optimizer [KB15] will be considered during training, but in some cases, we will switch to the LBFGS optimizer [SY06] at the n_{switch} -th epoch.

Once this network is defined, solving the PDE can be rewritten as a minimization problem on θ , namely finding the optimal weights θ^* that satisfy the following minimization problem:

$$\theta^* = \underset{\theta}{\operatorname{argmin}} (\omega_r J_r(\theta) + \omega_b J_b(\theta) + \omega_{\text{data}} J_{\text{data}}(\theta)), \quad (6.2)$$

with ω_r , ω_b and ω_{data} some weights to balance the different terms of the loss function.

In (6.2), the loss function owns three terms: the residual loss function

$$J_r(\theta) = \int_{\mathcal{M}} \int_{\Omega} |\mathcal{L}(u_\theta(\boldsymbol{x}, \boldsymbol{\mu}); \boldsymbol{x}, \boldsymbol{\mu}) - f(\boldsymbol{x}, \boldsymbol{\mu})|^2 d\boldsymbol{x} d\boldsymbol{\mu}, \quad (6.3)$$

the boundary loss function

$$J_b(\theta) = \int_{\mathcal{M}} \int_{\partial\Omega} |u_\theta(\boldsymbol{x}, \boldsymbol{\mu}) - g(\boldsymbol{x}, \boldsymbol{\mu})|^2 d\boldsymbol{x} d\boldsymbol{\mu}, \quad (6.4)$$

and the data loss function

$$J_{\text{data}}(\theta) = \frac{1}{N_{\text{data}}} \sum_{i=1}^{N_{\text{data}}} |u_\theta(\boldsymbol{x}_{\text{data}}^{(i)}, \boldsymbol{\mu}_{\text{data}}^{(i)}) - u_{\text{data}}^{(i)}|^2, \quad (6.5)$$

where $(\boldsymbol{x}_{\text{data}}^{(i)}, \boldsymbol{\mu}_{\text{data}}^{(i)}, u_{\text{data}}^{(i)})_{i=1, \dots, N_{\text{data}}}$ are N_{data} known data points with $u_{\text{data}}^{(i)}$ a reference solution at point $\boldsymbol{x}_{\text{data}}^{(i)}$ and for parameters $\boldsymbol{\mu}_{\text{data}}^{(i)}$.

Remark 14. These reference solutions can be the exact solutions of the parametric PDE, in this case, defined by $u_{\text{data}}^{(i)} = u(\boldsymbol{x}_{\text{data}}^{(i)}; \boldsymbol{\mu}_{\text{data}}^{(i)})$. They can also be an approximation produced by a numerical method, such as finite elements on a fine mesh.

Remark 15. In Section 8, the focus is on PINNs trained only on residual loss (with boundary conditions imposed exactly as presented in Section 6.2.1). We will only consider BC loss in Section 8.4.3. Furthermore, we will not use loss data in PINNs except in Section 8.2 where we will seek to compare a full PINN to a network trained only on data.

Solving the minimization problem (6.2) requires computing the gradient of the loss function with respect to θ , which involves calculating the integrals in (6.3) and (6.4). The most natural idea is to estimate them with a Monte-Carlo method, see e.g. [Caf98]. One could also use Gauss-type quadrature rules to evaluate integrals, as is done in Variational Physics-Informed Neural Networks [KZK21], but the limitation is the impossibility of selecting an adequate quadrature order due to the unknown properties of the Neural Network approximation. For

that purpose, we define so-called ‘‘collocation points’’ on $\Omega \times \mathcal{M}$ and its boundary $\partial\Omega \times \mathcal{M}$, denoted respectively by $(\mathbf{x}_{\text{col}}^{(i)}, \boldsymbol{\mu}_{\text{col}}^{(i)})_{i=1, \dots, N_{\text{col}}}$ and $(\mathbf{x}_{\text{bc}}^{(i)}, \boldsymbol{\mu}_{\text{bc}}^{(i)})_{i=1, \dots, N_{\text{bc}}}$. Then, we approximate the residuals and boundary losses by

$$J_r(\theta) \simeq \frac{1}{N_{\text{col}}} \sum_{i=1}^{N_{\text{col}}} |\mathcal{L}(u_\theta(\mathbf{x}_{\text{col}}^{(i)}, \boldsymbol{\mu}_{\text{col}}^{(i)}); \mathbf{x}_{\text{col}}^{(i)}, \boldsymbol{\mu}_{\text{col}}^{(i)}) - f(\mathbf{x}_{\text{col}}^{(i)}, \boldsymbol{\mu}_{\text{col}}^{(i)})|^2$$

and

$$J_b(\theta) \simeq \frac{1}{N_{\text{bc}}} \sum_{i=1}^{N_{\text{bc}}} |u_\theta(\mathbf{x}_{\text{bc}}^{(i)}, \boldsymbol{\mu}_{\text{bc}}^{(i)}) - g(\mathbf{x}_{\text{bc}}^{(i)}, \boldsymbol{\mu}_{\text{bc}}^{(i)})|^2.$$

Remark 16. *The values of N_{col} and N_{bc} are heuristically determined and should be large enough to ensure that the Monte-Carlo integration is accurate enough. The precise values of these parameters will be given in the numerical experiments.*

Remark 17. *In the case of complex geometries, one solution for obtaining a sample of points in the Ω domain is to use a level-set function, denoted φ . This function, which vanishes on the boundary of Ω , can be obtained differently. The authors of [SS22] propose different approaches to obtain a level-set function analytically in the case of polygonal or curved geometries. Learning-based approaches have also been proposed, notably in e.g. [PFS⁺19, SMB⁺20].*

Because of the minimization problem (6.2), the PINN u_θ does not exactly satisfy the boundary conditions. Moreover, loss functions compete, which may require fine-tuning the coefficients between J_r and J_b . In addition, classical PINNs do not include information on higher-order derivatives. As highlighted in Remarks 8 and 11, for our purposes, a good prior should yield a good approximation of the derivatives of the solution. For these reasons, the following section recalls several improvements of classical PINNs in the literature.

6.2 Improving PINN training and prediction

This section focuses on several ways of improving PINNs: exactly imposing the boundary conditions in Section 6.2.1, adding a higher-order derivative term in the loss function in Section 6.2.2, and countering the spectral bias in Section 6.2.3. Although these approaches are presented separately, they can easily be combined with one another.

6.2.1 Exact imposition of boundary conditions

To avoid the issues of classical PINNs discussed in Section 6.1, the authors of [LLF98, FMDN24] propose a method to enforce inhomogeneous Dirichlet boundary conditions exactly. To that end, they search the approximation u_θ of solution to (6.1) with the form: for all $\mathbf{x} \in \Omega$ and $\boldsymbol{\mu} \in \mathcal{M}$

$$u_\theta(\mathbf{x}, \boldsymbol{\mu}) = \varphi(\mathbf{x})w_\theta(\mathbf{x}, \boldsymbol{\mu}) + g(\mathbf{x}, \boldsymbol{\mu}),$$

where φ and w_θ are, respectively, the level-set function and a neural network as defined in Section 6.1. Thus u_θ will automatically satisfies the boundary conditions, since $u_\theta(\mathbf{x}, \boldsymbol{\mu}) = g(\mathbf{x}, \boldsymbol{\mu})$ for all $\mathbf{x} \in \partial\Omega$ and $\boldsymbol{\mu} \in \mathcal{M}$.

Remark 18. *Note that this level-set function can be used in a few different ways, firstly to generate a sample of points in Ω , as shown in Section 6.1, and secondly to impose boundary conditions. However, to use it directly in the formulation of the prior, it will require a certain regularity. For example, the signed distance function is not a good candidate.*

In this case, only the residual and data loss functions are minimized, and the minimization problem (6.2) becomes

$$\theta^* = \underset{\theta}{\operatorname{argmin}} (\omega_r J_r(\theta) + \omega_{\text{data}} J_{\text{data}}(\theta)),$$

with ω_r and ω_{data} some weights to balance the terms of the loss function.

Remark 19. *Similar methods exist for Robin and Neumann conditions; see [SS22].*

6.2.2 Sobolev training for PINNs

As presented in [Section 6.1](#), PINNs approximate the PDE solution by directly incorporating the equations into their training. Despite their effectiveness, these models can sometimes struggle to learn correctly, especially when the solution or its derivatives are complicated. The authors of [\[SJHH21\]](#) have proposed an approach called Sobolev training to try and overcome these difficulties. This method simply imposes constraints not only on the solutions themselves, but also on their derivatives. In the context of solving the problem [\(6.1\)](#) under consideration, Sobolev training is applied by adding a cost term J_{sob} to the initial minimization problem [\(6.2\)](#):

$$\theta^* = \underset{\theta}{\operatorname{argmin}} \left(\omega_r J_r(\theta) + \omega_{\text{sob}} J_{\text{sob}}(\theta) + \omega_b J_b(\theta) + \omega_{\text{data}} J_{\text{data}}(\theta) \right), \quad (6.6)$$

with J_r , J_b and J_{data} defined as in [\(6.3\)](#), [\(6.4\)](#) and [\(6.5\)](#) respectively and ω_r , ω_{sob} , ω_b and ω_{data} the weights to balance the different terms of the loss function. The Sobolev loss function J_{sob} in [\(6.6\)](#) is defined by

$$J_{\text{sob}}(\theta) = \int_{\mathcal{M}} \int_{\Omega} |\nabla_{\mathbf{x}}(\mathcal{L}(u_{\theta}(\mathbf{x}, \boldsymbol{\mu}); \mathbf{x}, \boldsymbol{\mu}) - f(\mathbf{x}, \boldsymbol{\mu}))|^2 d\mathbf{x}d\boldsymbol{\mu}, \quad (6.7)$$

where the integral is estimated by the Monte-Carlo method, similar to the other loss functions.

6.2.3 Overcoming the spectral bias

Multiple ways of overcoming the spectral bias of MLPs are available. For instance, in [\[TS20\]](#), the authors introduce Fourier features to improve the network, while the authors of [\[DHMM24\]](#) rely on a domain decomposition-based approach.

In this work, when dealing with high-frequency solutions (i.e., solutions with more than three wavelengths propagating), we use the Fourier features from [\[TS20\]](#). It relies on modifying the input of the neural network. Indeed, the prior u_{θ} is now defined, for all $\mathbf{x} \in \Omega$ and $\boldsymbol{\mu} \in \mathcal{M}$, as

$$u_{\theta}(\mathbf{x}, \boldsymbol{\mu}) = w_{\theta}(\mathbf{x}, \boldsymbol{\mu}; \sin(\pi a_1 \mathbf{x}), \cos(\pi b_1 \mathbf{x}), \dots, \sin(\pi a_{n_f} \mathbf{x}), \cos(\pi b_{n_f} \mathbf{x})),$$

where the $2n_f$ real numbers $(a_l)_{l \in \{1, \dots, n_f\}}$ and $(b_l)_{l \in \{1, \dots, n_f\}}$ are additional trainable parameters. This makes it possible to learn higher-frequency solutions, by also learning the frequency itself.

Remark 20. *This MLP with Fourier features (MLP w/ FF) needs the same parameters as the classical MLP (defined in [Remark 13](#)), but also the number of Fourier features n_f .*

7 Implementation details

Before moving on to numerical experiments, we discuss some practical details regarding the implementation of the methods introduced in [Sections 3](#) and [4](#). In [Section 7.1](#), we first look at how to effectively plug the PINN prediction in the FEM solver. Then, in [Section 7.2](#), we discuss the imposition of boundary conditions in the two proposed methods.

The tools used to implement the methods and obtain the results in [Section 8](#) are, on the one hand, `PyTorch` [\[Pea19\]](#) and `ScimBa` for the construction of the prior, in particular the implementation of PINN, and, on the other hand, `FEniCS` for the implementation of the finite element methods. For mesh generation, use either `FEniCS` or `mshr` mesh generators.

Remark 21. *In section [Section 8](#), we will not specify the training times of the networks, independently for each test case. To give an order of importance, PINN training takes less than ten minutes on a laptop GPU. For cases using the LFBGs optimizer, training takes a little longer, but still less than an hour.*

Remark 22. *Note that, `FEniCS` defines the characteristic mesh size h as the length of the longest edge, for $d \in \{1, 2\}$.*

7.1 Using PINN prediction effectively

To be effective, our methods will in practice depend on the quality of the approximation of the prior's derivatives, computed from automatic differentiation, and its precise integration on the domain.

Automatic differentiation. It is important to use the automatic differentiation offered by neural networks, enabling exact (in the sense of machine precision) derivative computation without having to manipulate complex symbolic expressions. In particular, in the context of PINNs, automatic differentiation will play a fundamental role in integrating the PDE under consideration. This automatic differentiation will enable the two improved finite element methods to use the exact derivatives of the prior u_θ and thus avoid introducing an additional error in the computation of the derivative.

Analytical function integration. Analytical functions in the weak problem must be integrated with sufficient precision for these approaches to be effective. Thus, in e.g. the additive approach, a quadrature rule with a higher degree than the traditional FEM has to be applied to discretize the term $l(v_h) - a(u_\theta, v_h)$ in (3.3). This point, and the required degree of the quadrature rule, will be studied in more detail in the first 2D test case considered in Section 8.4.1.5.

Remark 23. *In practice, the source term in the additive approach will be computed in the strong way. For instance, in the case of the Laplacian equation with $u_\theta = 0$ on $\partial\Omega$, the term*

$$l(v_h) - a(u_\theta, v_h) = \int_{\Omega} f v_h - \int_{\Omega} \nabla u_\theta \cdot \nabla v_h$$

will be replaced by

$$\int_{\Omega} (f + \Delta u_\theta) v_h.$$

If u_θ is not equal to zero on $\partial\Omega$, one needs to include a boundary term.

7.2 Imposing boundary conditions

In this section, we focus on the crucial question of imposing boundary conditions. We first look at this problem in the context of the additive approach presented in Section 3 and then in the context of the multiplicative approach presented in Section 4.

Remark 24. *For simplicity, this section focuses on (non-homogeneous) Dirichlet conditions. For our enhanced FEM, just like in classical FEM, these boundary conditions are imposed by manually eliminating essential dofs, see [EG04], and more precisely by modifying the matrix and the right-hand side of the linear system. This approach is not needed for Neumann and Robin conditions.*

7.2.1 Additive approach

In this first approach, if our Dirichlet problem satisfies $u = g$ on $\partial\Omega$, then p_h^+ has to satisfy

$$p_h^+ = g - u_\theta \quad \text{on } \partial\Omega,$$

with u_θ the PINN prior. This non-homogeneous boundary condition becomes homogeneous as soon as u_θ is exact at the boundary, or, in other words, as soon as the boundary conditions are imposed exactly in the PINN, as presented in Section 6.2.1.

Remark 25. *However, in the case of curved geometries (e.g. disks) where the meshes do not coincide with the boundary of the geometry, problems occur when $q > 2$, and especially on coarse meshes. In the numerical results, to avoid this problem and check the error estimates, we assume that $g = u$ on $\partial\Omega_h$ where Ω_h is the domain covered by the mesh. Furthermore, we need to be careful because even if, in PINN, the conditions are imposed exactly (as shown in Section 6.2.1), the prediction u_θ will not be exact on $\partial\Omega_h$. We made this choice here to simplify the problem, but in practice, solutions exist to improve the quality of the results.*

7.2.2 Multiplicative approach

In this second method, the boundary conditions are a bit more complex to handle. In the [Section 4](#), we have denoted by

$$u_{h,M}^\times = u_{\theta,M} p_h^\times$$

the solution obtained by the multiplicative approach to the modified problem (4.1) with the prior $u_{\theta,M} = u_\theta + M$. Therefore, we can recover the solution u_h^\times of the original problem (1.1) by setting $u_h^\times = u_{h,M}^\times - M$.

Standard PINN. In the case where our prior u_θ is the prediction of a standard PINN, as presented in [Section 6.1](#), the boundary conditions are not imposed exactly. Thus, if our problem satisfies $u = g$ on $\partial\Omega$, then p_h^\times has to satisfy

$$p_h^\times = \frac{g + M}{u_{\theta,M}} \quad \text{on } \partial\Omega.$$

PINN with exact BC. We now focus on the case where we exactly impose the boundary conditions in the PINN, as presented in [Section 6.2.1](#). Then, supposing that $M > 0$, we have $u_{\theta,M} = g + M$ on $\partial\Omega$ and therefore p_h^\times has to satisfy

$$p_h^\times = 1 \quad \text{on } \partial\Omega.$$

However, there is a specific case when this condition is not necessarily true. Indeed, if the boundary conditions are homogeneous, then $g = 0$ and $u_{\theta,M} = M$ on $\partial\Omega$. Considering that $u_\theta > 0$ in Ω , $M = 0$ is a possible choice. In this case, $u_{\theta,M} = u_{\theta,0} = 0$ on $\partial\Omega$, and $u_{h,M}^\times = u_{h,0}^\times = u_h^\times$ automatically satisfies the boundary conditions. Hence, imposing a boundary condition on p_h^\times becomes unnecessary.

Remark 26. *In the numerical results of [Section 8.3](#), one of these specific cases is considered in 1D. We will see that leaving p_h^\times free will give better results here than imposing $p_h^\times = 1$ on $\partial\Omega$. Indeed, this approach leaves more freedom to capture the correct derivatives at the boundary.*

8 Numerical results

This section is dedicated to validating the proposed method on several numerical experiments, which are instances of the problem (1.1) presented in [Section 1](#) with spatial dimension $d \in \{1, 2\}$, and with increasing complexity. The idea is to compare, in different ways, the additive and multiplicative approaches presented in [Section 3](#) and [Section 4](#) to the standard finite element method presented in [Section 2](#). The multiplicative approach will only be considered in dimension $d = 1$, showing that only in rare cases, and with a good choice of the lifting constant M , does it provide better results than the additive one. We will also show that the approach proposed in [Section 6](#) for choosing the prior is more efficient than more classical ones, considering the 1D case.

In [Section 8.1](#), we present the two tests that will be performed for each test case. We are interested in two 1D test cases ($d = 1$): the Poisson problem with homogeneous Dirichlet conditions in [Section 8.2](#) and a general elliptic system and convection-dominated regime problem in [Section 8.3](#). We then consider two 2D cases ($d = 2$): We start with a Poisson problem with homogeneous Dirichlet conditions on a square domain in [Section 8.4](#). We then continue with a slightly more complicated elliptic problem, still with Dirichlet conditions and on a square domain, in [Section 8.5](#). In [Section 8.6](#), we return to the 2D Poisson problem, but this time considering mixed boundary conditions on a ring-shaped domain.

The implementation of the numerical results obtained on the various test cases is available at the following address:

<https://github.com/flecourtier/EnrichedFEMUsingPINNs>.

8.1 Setup of the numerical experiments

For each of the proposed test cases, we consider a parametric problem, on which we train a PINN as presented in [Section 6.1](#), to resolve it on a set of fixed parameters, denoted by \mathcal{M} . Let $p = \dim(\mathcal{M})$ be the number of parameters, and consider a sample \mathcal{S} of n_p parameters:

$$\mathcal{S} = \left\{ \boldsymbol{\mu}^{(1)}, \dots, \boldsymbol{\mu}^{(n_p)} \right\},$$

with, for $j = 1, \dots, n_p$,

$$\boldsymbol{\mu}^{(j)} = \left(\mu_1^{(j)}, \dots, \mu_p^{(j)} \right) \in \mathcal{M}.$$

In the following, we denote by $u^{(j)}$ a reference solution to problem [\(6.1\)](#) for a given parameter $\boldsymbol{\mu}^{(j)}$ and by $u_h^{(j)}$ the solution obtained by the standard finite element method [\(2.3\)](#) where V_h is the \mathbb{P}_k Lagrange space defined in [\(2.2\)](#) and h is the characteristic mesh size. We also denote by $u_\theta^{(j)}$ the solution obtained by the parametric PINN, and by $u_{h,+}^{(j)}$ the solution obtained by the additive approach [\(3.3\)](#) with V_h^+ the \mathbb{P}_k Lagrange space defined in [\(3.1\)](#). In some test cases, we also consider the solution $u_{h,M}^{(j)}$ of the multiplicative approach [\(4.4\)](#) with V_h^\times the \mathbb{P}_k Lagrange space defined in [\(4.3\)](#), depending on the lifting constant M .

Remark 27. *In the following, to estimate the error, we consider the reference solution to be either an analytical solution or a solution obtained with a very fine mesh and a high polynomial degree. More precisely, we need the characteristic size h_{ref} associated with the reference mesh to be much smaller than the size associated with the current mesh h , i.e. $h_{\text{ref}} \ll h$, and we will consider $k_{\text{ref}} = 3$ the polynomial degree associated with the reference solution.*

In each test case, we investigate two aspects; the first in [Section 8.1.1](#) involves verifying the error estimates and the second in [Section 8.1.2](#) is the evaluation of the gains achieved by the proposed methods compared with the standard one.

8.1.1 Error estimates

Consider a small sample \mathcal{S} with $n_p = 2$ parameters. Given a fixed parameter $\boldsymbol{\mu}^{(j)}$, $j = 1, 2$, we start by testing the error estimates obtained in [Theorem 6](#) for the additive approach. In the case $d = 1$, we will also be interested in the error estimates in [Theorem 9](#) for the multiplicative approach. By varying the mesh size h , we then estimate the errors obtained with the two methods. To evaluate these errors, we compare the approximations to the reference solution $u^{(j)}$ (see [Remark 27](#)). We then define by

$$e_h^{(j)} = \frac{\|u^{(j)} - u_h^{(j)}\|_{L^2}}{\|u^{(j)}\|_{L^2}} \quad \text{and} \quad e_\theta^{(j)} = \frac{\|u^{(j)} - u_\theta^{(j)}\|_{L^2}}{\|u^{(j)}\|_{L^2}} \quad (8.1)$$

the L^2 relative error obtained for the standard FEM and the PINN respectively. We further define,

$$e_{h,+}^{(j)} = \frac{\|u^{(j)} - u_{h,+}^{(j)}\|_{L^2}}{\|u^{(j)}\|_{L^2}} \quad \text{and} \quad e_{h,M}^{(j)} = \frac{\|u^{(j)} - u_{h,M}^{(j)}\|_{L^2}}{\|u^{(j)}\|_{L^2}} \quad (8.2)$$

the L^2 relative errors obtained for the additive and multiplicative approach (depending on the lifting constant M), respectively.

8.1.2 Gains achieved with the enriched bases

As we have trained the network to be parameter-dependent to predict a solution for a set of parameters, we are interested in the average gains we obtain with our enriched approaches compared to the PINN and the standard FEM. More precisely, for a fixed mesh size h and a fixed polynomial degree k , for a sample \mathcal{S} of n_p parameters,

the numerical gains obtained by the additive approach on PINN and standard FEM are respectively defined for $j = 1, \dots, n_p$ by:

$$G_{+, \theta}^{(j)} = \frac{e_{\theta}^{(j)}}{e_{h,+}^{(j)}} \quad \text{and} \quad G_{+}^{(j)} = \frac{e_h^{(j)}}{e_{h,+}^{(j)}}, \quad (8.3)$$

with $e_{\theta}^{(j)}$, $e_h^{(j)}$ and $e_{h,+}^{(j)}$ respectively the L^2 relative errors obtained with the PINN, the standard FEM and the additive approach, defined in [Section 8.1.1](#). Similarly, the theoretical gains obtained by the multiplicative approach (depending on the lifting constant M) on PINN and standard FEM are respectively defined for $j = 1, \dots, n_p$ by:

$$G_{M, \theta}^{(j)} = \frac{e_{\theta}^{(j)}}{e_{h,M}^{(j)}} \quad \text{and} \quad G_M^{(j)} = \frac{e_h^{(j)}}{e_{h,M}^{(j)}}, \quad (8.4)$$

with $e_{h,M}^{(j)}$ the L^2 relative error obtained with the multiplicative approach (depending on the lifting constant M), defined in [Section 8.1.1](#). Therefore, we will be interested in the minimum, maximum, mean and standard deviation obtained on the following samples :

$$G_{+, \theta} = \left\{ G_{+, \theta}^{(1)}, \dots, G_{+, \theta}^{(n_p)} \right\} \quad \text{and} \quad G_{+} = \left\{ G_{+}^{(1)}, \dots, G_{+}^{(n_p)} \right\}, \quad (8.5)$$

which respectively represent the gains obtained with our additive approach over PINNs and over standard FEM on the sample \mathcal{S} . In the same way, we define $G_{M, \theta}$ and G_M , which respectively represent the gains obtained with our multiplicative approach over PINN and over standard FEM on the sample \mathcal{S} by:

$$G_{M, \theta} = \left\{ G_{M, \theta}^{(1)}, \dots, G_{M, \theta}^{(n_p)} \right\} \quad \text{and} \quad G_M = \left\{ G_M^{(1)}, \dots, G_M^{(n_p)} \right\}. \quad (8.6)$$

8.2 1D Poisson problem

In this section, we will consider the problem (1.1) in its most simplified Poisson form, with homogeneous Dirichlet boundary conditions. In the 1D case ($d = 1$), we have,

$$\begin{cases} -\partial_{xx} u = f, & \text{in } \Omega \times \mathcal{M}, \\ u = 0, & \text{on } \partial\Omega \times \mathcal{M}, \end{cases} \quad (8.7)$$

with $\Omega = [0, 1]$, $\partial\Omega$ its boundary and $\mathcal{M} \subset \mathbb{R}^p$ the parameter space (with p the number of parameters). For this problem, we consider solutions defined with $p = 3$ parameters $\boldsymbol{\mu} = (\mu_1, \mu_2, \mu_3) \in \mathcal{M} = [0, 1]^3$ defined by

$$u(x; \boldsymbol{\mu}) = \mu_1 \sin(2\pi x) + \mu_2 \sin(4\pi x) + \mu_3 \sin(6\pi x).$$

Note that the associated right-hand side f in (8.7) also depends on $\boldsymbol{\mu}$. This problem is thus four-dimensional: one dimension in space and three dimensions for the parameters $\boldsymbol{\mu}$.

For this first test case, we construct two priors, as detailed in [Section 8.2.1](#). The first one, denoted by u_{θ} , is built from a PINN as presented in [Section 6](#). The second one, denoted by u_{θ}^{data} is constructed only from data (obtained from the analytical solution). The aim is to show that using physics-informed training to construct the prior leads to better results than data-driven training. In this test case, we also compare the additive and multiplicative approaches (presented for several values of M), but only with $k = 1$ polynomial order to remain concise.

We first present the error estimates obtained with the PINN prior in [Section 8.2.2](#). First, we check the orders of convergence of the two enriched approaches. Then, we verify the results expected in [Section 5](#) by comparing the theoretical gain constants of the additive and multiplicative approaches. Afterwards, in [Section 8.2.3](#), we compare, for a given parameter, the derivatives obtained with the two priors and analyze the associated gains. Finally, we evaluate the gains obtained with the two priors in [Section 8.2.4](#) on a sample of parameters.

Remark 28. In the following, the characteristic mesh size $h = \frac{1}{N-1}$, where N represents the number of considered nodes.

8.2.1 Construction of the two priors

The hyperparameters used to construct the two priors are presented in [Table 1](#). We discuss below the specific differences in training both priors.

Network - MLP		Training		Loss weights			
<i>layers</i>	20, 80, 80, 80, 20, 10	<i>lr</i>	9e-2	PINN prior u_θ		Data prior u_θ^{data}	
σ	sine	<i>decay</i>	0.99	ω_r	1	ω_{data}	0
		<i>n_{epochs}</i>	10000	ω_r	0	ω_{data}	1
		N_{col} or N_{data}	5000	ω_b	0	ω_{sob}	0

Table 1: Network, training parameters ([Remark 13](#)) and loss weights for u_θ and u_θ^{data} in the *1D Poisson problem*. Considering N_{col} collocation points for the PINN prior and N_{data} data for the data prior.

Physics-informed training. For the first prior, we will consider a parametric PINN, depending on the problem parameters $\boldsymbol{\mu}$, where we exactly impose the Dirichlet boundary conditions as presented in [Section 6.2.1](#) and without using data in training. We define the prior

$$u_\theta(x, \boldsymbol{\mu}) = \varphi(x)w_\theta(x, \boldsymbol{\mu}), \quad (8.8)$$

where w_θ is the neural network under consideration and φ is the level-set function defined by

$$\varphi(x) = x(x - 1), \quad (8.9)$$

which vanishes exactly on $\partial\Omega$. Since we impose the boundary conditions by using the level-set function, we will only consider the residual loss J_r defined in [\(6.3\)](#) in which the integrals are approached by a Monte-Carlo method, i.e.

$$J_r(\theta) \simeq \frac{1}{N_{\text{col}}} \sum_{i=1}^{N_{\text{col}}} |\partial_{xx} u_\theta(\mathbf{x}_{\text{col}}^{(i)}; \boldsymbol{\mu}_{\text{col}}^{(i)}) + f(\mathbf{x}_{\text{col}}^{(i)}; \boldsymbol{\mu}_{\text{col}}^{(i)})|^2$$

with the $N_{\text{col}} = 5000$ collocation points $(\mathbf{x}_{\text{col}}^{(i)}, \boldsymbol{\mu}_{\text{col}}^{(i)})_{i=1, \dots, N_{\text{col}}}$ uniformly chosen on $\Omega \times \mathcal{M}$. Thus, we seek to solve the following minimisation problem

$$\theta^* = \underset{\theta}{\operatorname{argmin}} J_r(\theta).$$

In this first case, we consider an MLP with 6 layers and a sine activation function. The hyperparameters are given in [Table 1](#); we use the Adam optimizer [[KB15](#)].

Data-driven training. For the second prior considered, noted u_θ^{data} , a network is trained only on the data (constructed from the analytical solution). In this second case, we still consider the parameters defined in [Table 1](#), which are the same as for the physics-informed training except that we take $N_{\text{data}} = 5000$ instead of $N_{\text{col}} = 5000$. Considering, for each epoch, a set of parameters and points $(\mathbf{x}_{\text{data}}^{(i)}, \boldsymbol{\mu}_{\text{data}}^{(i)})_{i=1, \dots, N_{\text{data}}}$, the data loss is defined by

$$J_{\text{data}}(\theta) = \frac{1}{N_{\text{data}}} \sum_{i=1}^{N_{\text{data}}} |u_\theta^{\text{data}}(\mathbf{x}_{\text{data}}^{(i)}; \boldsymbol{\mu}_{\text{data}}^{(i)}) - u(\mathbf{x}_{\text{data}}^{(i)}; \boldsymbol{\mu}_{\text{data}}^{(i)})|^2,$$

and thus we seek to solve the following minimisation problem

$$\theta^* = \underset{\theta}{\operatorname{argmin}} J_{\text{data}}(\theta).$$

Remark 29. As for the PINN prior, we impose the boundary conditions exactly in the data-driven training.

8.2.2 Error estimates — with the PINN prior

In this section, we look at the theoretical results of the additive and multiplicative approaches, considering the PINN prior u_θ . First, we check the orders of convergence of [Theorems 6](#) and [9](#) (in the L^2 norm), associated with both methods. Next, we numerically verify [Theorem 12](#), showing that the multiplicative correction converges, for sufficiently large M , towards the additive correction (in both the L^2 norm and H^1 semi-norm).

Convergence rate. We test the error estimates of [Theorems 6](#) and [9](#) for the following two sets of parameters:

$$\boldsymbol{\mu}^{(1)} = (0.3, 0.2, 0.1) \quad \text{and} \quad \boldsymbol{\mu}^{(2)} = (0.8, 0.5, 0.8), \quad (8.10)$$

with the PINN prior u_θ . For $j \in \{1, 2\}$, the aim is to compare, by varying the mesh size h , the L^2 relative errors $e_h^{(j)}$ obtained with the standard FEM, defined in (8.1), $e_{h,+}^{(j)}$ obtained with the additive approach, defined in (8.2) and $e_{h,M}^{(j)}$ obtained with the multiplicative approach (taking $M = 3$ and $M = 100$), defined in (8.2). The results are presented in [Figure 2](#) for a polynomial orders $k = 1$ and $k = 2$, with h depending on the number of nodes $N \in \{16, 32, 64, 128, 256\}$ as presented in [Remark 28](#).

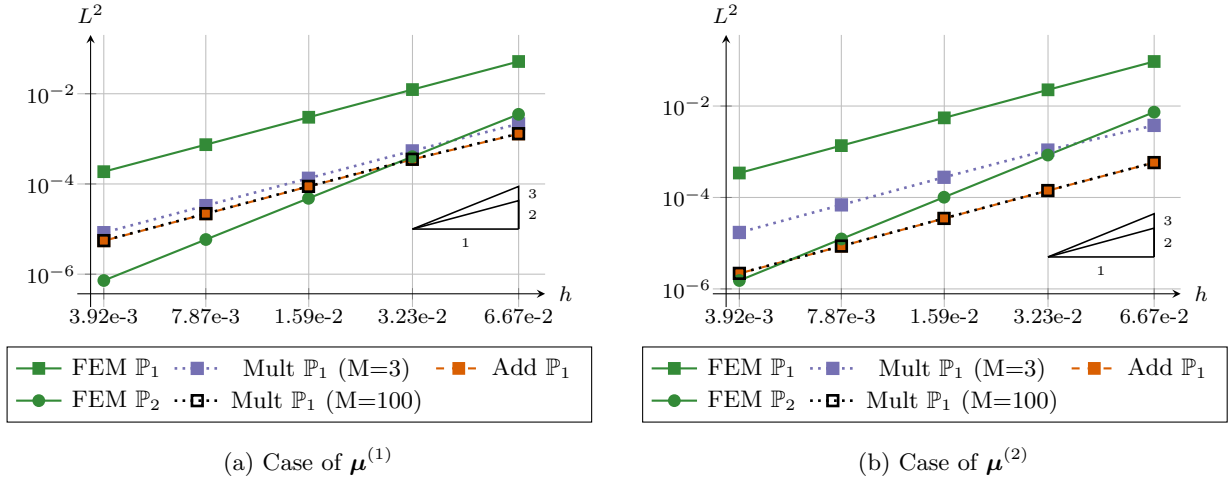


Figure 2: Considering the $1D$ Laplacian case and the PINN prior u_θ . Left – Considering $\boldsymbol{\mu}^{(1)}$. L^2 error on h obtained with standard FEM $e_h^{(1)}$ (solid lines) with $k = 1$ and $k = 2$, the additive approach $e_{h,+}^{(1)}$ (dashed lines) with $k = 1$ and the multiplicative approach $e_{h,M}^{(1)}$ (dotted lines), with $k = 1$ ($M = 3$ and $M = 100$). Right – Same for $\boldsymbol{\mu}^{(2)}$.

The results of [Figure 2](#) show that all the enriched finite elements increase the accuracy of the method and that they also converge at the same rate as the classical approach (i.e., as for the polynomial approximation order $k = 1$). Furthermore, the theoretical analysis (which showed that the multiplicative correction has the same error as the additive one when $M \rightarrow \infty$) is confirmed for both sets of parameters. In addition, [Figure 2](#) also shows that this multiplicative enrichment can be less efficient for small M when the $(k + 1)^{\text{th}}$ derivative of the solution is large. Indeed, for the first parameter considered in [Figure 2a](#), for which the second derivative takes lower values, we observe that the multiplicative approach with small M is closer to the additive one than for the second set of parameters considered in [Figure 2b](#), for which the derivatives are larger. Moreover, it seems that we gain almost one order of interpolation with the additive approach: in [Figure 9](#), the additive method with polynomial order $k = 1$ gives an error L^2 close to the original FEM method with $k = 2$, although the rate of convergence is different.

Gain constants. We consider the first parameter $\boldsymbol{\mu}^{(1)}$ and the PINN prior u_θ . We now evaluate the gain constants C_{gain}^+ and $C_{\text{gain}}^{\times, M}$ (for different values of M), are respectively defined in [Remarks 7](#) and [10](#) for the additive and multiplicative approaches. The idea is to check the convergence of the multiplicative gain constant towards the additive one, as proven in [Theorem 12](#). The results are presented in [Figure 3](#) for L^2 and H^1 norms.

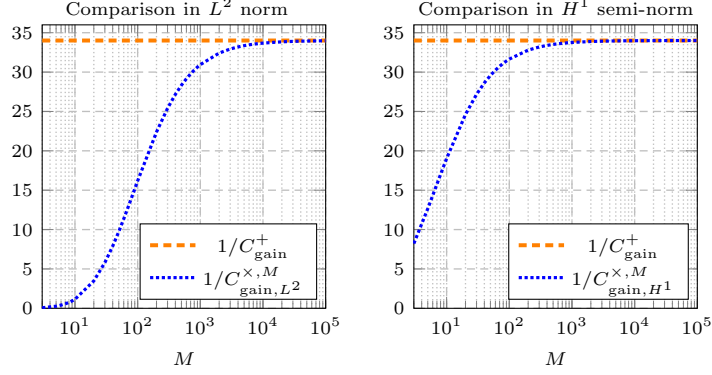


Figure 3: Considering the *1D Laplacian case* with $\mu^{(1)}$, $k = 1$ and the PINN prior u_θ . Left – Convergence of [Theorem 12](#) with the L^2 error. Right – Convergence of [Theorem 12](#) with the H^1 error.

[Figure 3](#) shows that the multiplicative gain constant converges to the additive gain constant when M increases, as expected in the theoretical results of [Theorem 12](#).

8.2.3 Derivatives — with both priors

To better explain the results of [Section 8.2.2](#), we compare the solution, the first- and second-order derivatives between the exact solution and the prediction of both priors, for selected parameter $\mu^{(1)}$. [Figures 4](#) and [5](#) respectively present this comparison for the PINN prior u_θ and the data prior u_θ^{data} . We also compare the errors and gains obtained with these two priors for $N \in \{16, 32\}$ in [Table 2](#). More precisely, we evaluate the additive error $e_{h,+}^{(1)}$ and the additive gain on FEM $G_+^{(1)}$, respectively defined in [\(8.2\)](#) and [\(8.3\)](#), for both PINN and data priors. We also evaluate the multiplicative error $e_{h,M}^{(1)}$ and the multiplicative gain on FEM $G_M^{(1)}$ defined in [\(8.2\)](#) and [\(8.4\)](#), for both priors, with $M = 3$ and $M = 100$.

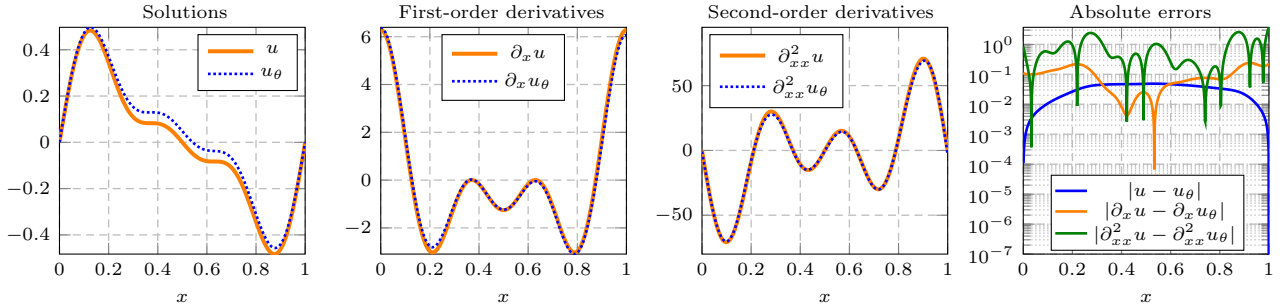


Figure 4: Considering the *1D Laplacian case* with $\mu^{(1)}$ and the PINN prior u_θ , comparison between analytical solution and network prediction. From left to right: solution; first derivative; second derivative; errors.

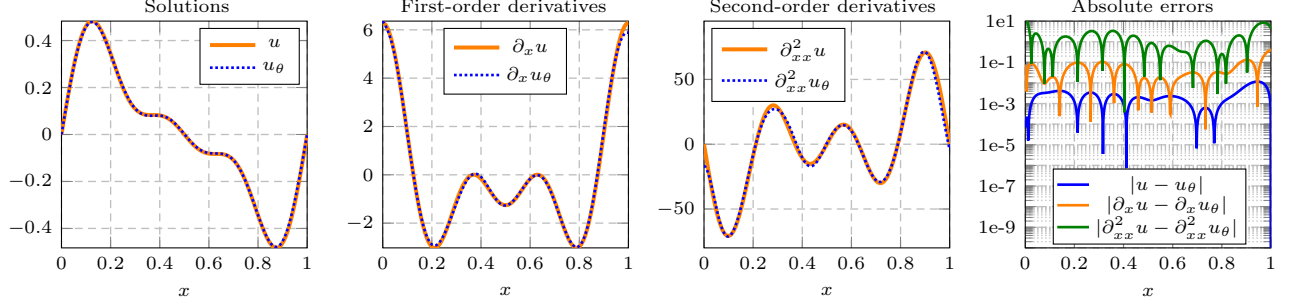


Figure 5: Considering the *1D Laplacian case* with $\mu^{(1)}$ and the data prior u_θ^{data} , comparison between analytical solution and network prediction. From left to right: solution; first derivative; second derivative; errors.

		PINN prior u_θ		Data prior u_θ^{data}		
		error	gain	error	gain	
N	FEM					
	error					
16	$5.18 \cdot 10^{-2}$					
32	$1.24 \cdot 10^{-2}$					
Add	N	16	$1.29 \cdot 10^{-3}$	40.34	$3.51 \cdot 10^{-3}$	14.78
	N	32	$3.49 \cdot 10^{-4}$	35.41	$8.8 \cdot 10^{-4}$	14.06
Mult (M=3)	N	16	$2.15 \cdot 10^{-3}$	24.13	$3.38 \cdot 10^{-3}$	15.36
	N	32	$5.41 \cdot 10^{-4}$	22.86	$8.53 \cdot 10^{-4}$	14.51
Mult (M=100)	N	16	$1.3 \cdot 10^{-3}$	39.84	$3.5 \cdot 10^{-3}$	14.83
	N	32	$3.53 \cdot 10^{-4}$	35.08	$8.78 \cdot 10^{-4}$	14.09

Table 2: Considering the *1D Laplacian case* with $\mu^{(1)}$, $k = 1$ and $N = 16, 32$. Left – L^2 relative error obtained with FEM. Right – Considering the PINN prior u_θ and the data prior u_θ^{data} , L^2 relative errors and gains with respect to FEM, obtained with our methods. Our methods : additive approach, multiplicative approach with $M = 3$ and $M = 100$.

The results reported in Figures 4 and 5 and Table 2 show that, even if the approach chosen to build the prior (physics-informed or data-driven training) gives a good approximation of the solution, the important point lies in the derivatives and mainly in the second-order derivatives, which are clearly better learned by PINNs. Indeed, while the enriched FEM solution is more accurate using the PINN prior (Table 2), we see from Figures 4 and 5 and Table 2 that the raw PINN approximates the solution u less accurately than the raw data-driven the solution, but the PINN better approximates the derivatives. As the error of the enriched FEM is mainly due to the $k + 1^{\text{th}}$ derivatives of the network being close to the $k + 1^{\text{th}}$ derivatives of the solution, this explains why the enriched FEM with data prior does not perform as well as with a PINN prior. Therefore, PINNs have two advantages: they do not require training data and give better results. Their main shortcoming is that training takes longer. However, we mention that if data are available for first- and second-order derivatives, it could also be used to improve a purely data-driven prior.

8.2.4 Gains achieved with the additive and multiplicative approaches – with both priors

Considering a sample \mathcal{S} of $n_p = 100$ parameters, we now evaluate the gains $G_{+, \theta}$ and G_+ defined in (8.5) with the PINN prior u_θ and with the data prior u_θ^{data} . We also compute $G_{M, \theta}$ and G_M , defined in (8.6), similarly for both priors. For fixed polynomial order $k = 1$ and $N \in \{20, 40\}$, the results with the physics-informed prior u_θ and the data-driven prior u_θ^{data} are respectively presented in Tables 3 and 4.

method	N	Gains in L^2 rel error of our method w.r.t. PINN				Gains in L^2 rel error of our method w.r.t. FEM			
		min	max	mean	std	min	max	mean	std
Add	20	10.47	251.6	92.19	50.96	26.49	271.92	140.74	55.16
	40	42.12	969.51	362.88	195.53	23.4	258.37	134.11	51.86
Mult (M=3)	20	5.19	106.29	25.34	20.57	3.93	163.81	42.72	34.93
	40	17.25	443.21	99.66	85.19	3.16	149.83	40.22	33.75
Mult (M=100)	20	10.48	253.57	92.59	51.9	26.29	270.87	140.82	55
	40	42.17	979.91	364.38	199.36	23.28	257.71	134.15	51.62

Table 3: Considering the *1D Laplacian case* and the PINN prior u_θ . Left – Gains in L^2 error of our methods with respect to PINN by taking $k = 1$. Right – Gains in L^2 error of our methods with respect to FEM by taking $k = 1$. Our methods : additive approach, multiplicative approach with $M = 3$ and $M = 100$.

method	N	Gains in L^2 rel error of our method w.r.t. Data Network				Gains in L^2 rel error of our method w.r.t. FEM			
		min	max	mean	std	min	max	mean	std
Add	20	1.34	10.95	3.33	2.09	6.91	60.85	26.12	12.45
	40	4.35	34.37	11.19	6.97	7.13	39.34	20.55	7.94
Mult (M=3)	20	0.85	10.4	2.56	1.98	3.54	53.99	19.66	11.11
	40	2.64	35.3	8.68	6.98	2.18	39.06	15.66	8.25
Mult (M=100)	20	1.35	10.96	3.33	2.09	6.9	60.73	26.11	12.43
	40	4.35	34.41	11.19	6.97	7.13	39.38	20.55	7.93

Table 4: Considering the *1D Laplacian case* and the Data prior v_θ^{data} . Left – Gains in L^2 error of our methods with respect to Data Network by taking $k = 1$. Right – Gains in L^2 error of our methods with respect to FEM by taking $k = 1$. Our methods : additive approach, multiplicative approach with $M = 3$ and $M = 100$.

The previous results indicate that the average gain provided by the enriched FE with the PINN prior is significant, particularly when using the additive approach. These findings also confirm the behaviour of the multiplicative prior method for varying values of M . In contrast, when applied with data-driven instead of physics-informed training, the same method does not yield similarly favourable results. Consequently, in the experiments we perform below, we only employ the PINN prior.

8.3 1D general elliptic system and convection-dominated regime

In this experiment, we consider the problem (1.1) in a more complex form, still in a 1D ($d = 1$) configuration:

$$\begin{cases} \partial_x u - \frac{1}{\text{Pe}} \partial_{xx} u = r, & \text{in } \Omega \times \mathcal{M}, \\ u = 0, & \text{on } \partial\Omega \times \mathcal{M}, \end{cases}$$

with $\Omega = [0, 1]$ and $\partial\Omega$ its boundary, r the reaction constant term and Pe the Péclet number which describe the ratio between convective and diffusion term. We define an analytical solution for all $x \in \Omega$ by

$$u(x; \boldsymbol{\mu}) = r \left(x - \frac{e^{\text{Pe}x} - 1}{e^{\text{Pe}} - 1} \right), \quad (8.11)$$

with $p = 2$ parameters $\boldsymbol{\mu} = (r, \text{Pe}) \in \mathcal{M} = [1, 2] \times [10, 100]$.

Remark 30. In large Péclet regime, i.e., for convection-dominated flows, the classical finite element method may generate oscillations when no specific treatment is applied, see e.g. [JKN18].

In this test-case, we will construct only one prior, denoted u_θ , built from a PINN as presented in Section 6. We will also compare the additive and multiplicative approaches by considering polynomial order $k = 1$, and since the solution is positive in Ω , we consider $M = 0$ for the multiplicative approach. We start by evaluating the error in Section 8.3.1, then we compare the derivatives of the PINN prior and compare the different approaches in Section 8.3.2. Finally, we evaluate the gains obtained in Section 8.3.3 on a sample of parameters. As we are dealing with a specific case, we will compare two methods for imposing boundary conditions, as presented in Section 7.2.2: the strong and the weak approaches.

Remark 31. As in Section 8.2, the characteristic mesh size $h = \frac{1}{N-1}$, where N is the number of nodes considered.

Physics-informed training. We consider a parametric PINN, depending on the problem parameters μ , where we exactly impose the Dirichlet boundary conditions as presented in Section 6.2.1. We define the prior u_θ and the level set φ as in (8.8) and (8.9), which vanishes exactly on $\partial\Omega$.

Network - MLP		Training		Loss weights					
<i>layers</i>	40, 40, 40, 40, 40	<i>lr</i>	1e-3	<i>decay</i>	0.99	ω_r	1	ω_{data}	0
σ	tanh	<i>n_{epochs}</i>	20000	ω_b	0	ω_{sob}	0		
		N_{col}	5000						

Table 5: Network, training parameters (Remark 13) and loss weights for u_θ in the 1D Elliptic case.

Since we impose the boundary conditions by using the level-set function, we will only consider the residual loss J_r defined in (6.3) in which the integrals are approached by a Monte-Carlo method, i.e.

$$J_r(\theta) \simeq \frac{1}{N_{\text{col}}} \sum_{i=1}^{N_{\text{col}}} \left| \partial_x u_\theta(\mathbf{x}_{\text{col}}^{(i)}; \boldsymbol{\mu}_{\text{col}}^{(i)}) - \frac{1}{\text{Pe}} \partial_{xx} u_\theta(\mathbf{x}_{\text{col}}^{(i)}; \boldsymbol{\mu}_{\text{col}}^{(i)}) - r \right|^2,$$

with the $N_{\text{col}} = 5000$ collocation points $(\mathbf{x}_{\text{col}}^{(i)}, \boldsymbol{\mu}_{\text{col}}^{(i)})_{i=1, \dots, N_{\text{col}}}$ uniformly chosen on $\Omega \times \mathcal{M}$. Thus we seek to solve the following minimisation problem

$$\theta^* = \underset{\theta}{\text{argmin}} J_r(\theta).$$

In this case, we consider a MLP with 5 layers and a tanh activation function. The hyperparameters are given in Table 5; we use the Adam optimizer [KB15].

8.3.1 Error estimates

We start by testing the error estimates (Theorem 6) for the following two sets of parameters:

$$\boldsymbol{\mu}^{(1)} = (1.2, 40) \quad \text{and} \quad \boldsymbol{\mu}^{(2)} = (1.5, 90), \quad (8.12)$$

by considering the PINN prior u_θ . For $j \in \{1, 2\}$, the aim is to compare for different mesh sizes h , the L^2 relative errors $e_h^{(j)}$ obtained with the standard FEM method, defined in (8.1), $e_{h,+}^{(j)}$ obtained with the additive approach and $e_{h,M}^{(j)}$ obtained with the multiplicative approach (taking $M = 0$), defined in (8.2). We will consider the two implementations of the boundary conditions for the multiplicative approach: the strong and the weak BC, as presented in Section 4. The results are presented in Figure 6 by varying the mesh size h .

In Figure 6, we see that the enriched approaches seem to give better results than standard FEM except for the multiplicative approach with strong imposition of boundary conditions. Moreover, this approach, which imposes $p_h^\times = 1$ on $\partial\Omega$, does not follow the expected convergence order. The additive approach seems much less effective

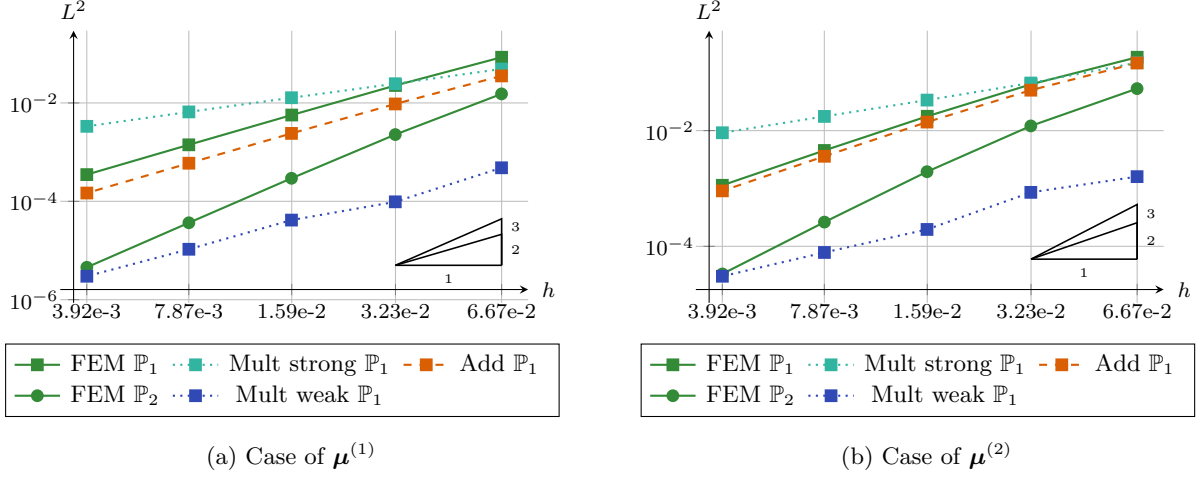


Figure 6: Considering the *1D Elliptic case* and the PINN prior u_θ . Left – Considering $\mu^{(1)}$. L^2 error on h obtained with standard FEM $e_h^{(1)}$ (solid lines) with $k = 1$ and $k = 2$, the additive approach $e_{h,+}^{(1)}$ (dashed lines) with $k = 1$ and the multiplicative approach $e_{h,M}^{(1)}$ (dotted lines) with $k = 1$, considering strong and weak BC. Right – Same for $\mu^{(2)}$, (8.12).

here than in the previous experiment of Section 8.2, whereas the multiplicative approach with weak BC seems to significantly improve the results obtained with standard FEM. A comparative study of the different methods is given in Section 8.3.2. In addition, we see that the standard FEM method with polynomial order $k = 2$ is clearly less accurate than the multiplicative approach using weak BC applied with polynomial order $k = 1$.

8.3.2 Comparison of different approaches

We now focus on the second parameter $\mu^{(2)}$. We first look at the PINN prediction for this parameter and its derivatives in Figure 7. As in the previous section, we consider the following approaches: standard FEM, the additive approach and the multiplicative approach (with $M = 0$) with strong or weak imposition of boundary conditions. We compare the different methods in Table 6, where we can see the different errors obtained with the considered methods for $k = 1$ and $N \in \{16, 32\}$ as well as the gains obtained in comparison with standard FEM. Next, we take a closer look at the solutions obtained with the different approaches in Figure 8; for each method, we compare the solution obtained (u_h for standard FEM, u_h^+ for the additive approach and u_h^\times for the multiplicative approach, with strong or weak BC imposition) with the analytical solution u . For the enriched methods, using the PINN prior, we will also compare the proposed correction; namely, for the additive approach, we will compare p_h^+ with $u - u_\theta$ and for the multiplicative one p_h^\times with u/u_θ (with $u_\theta > 0$ in Ω).

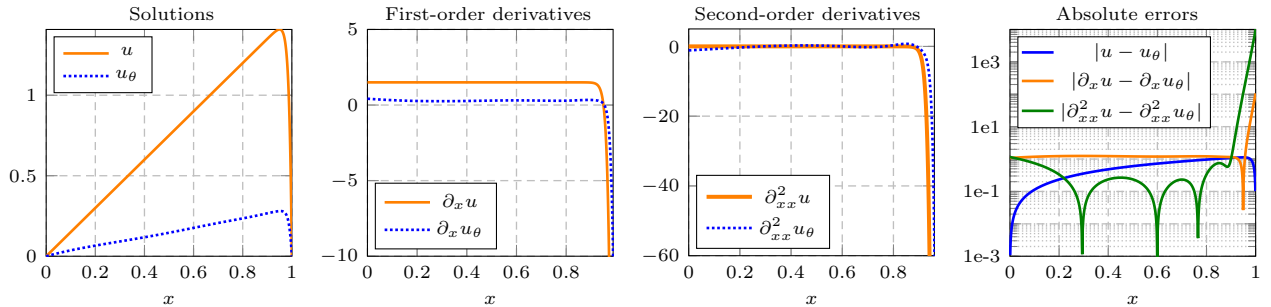
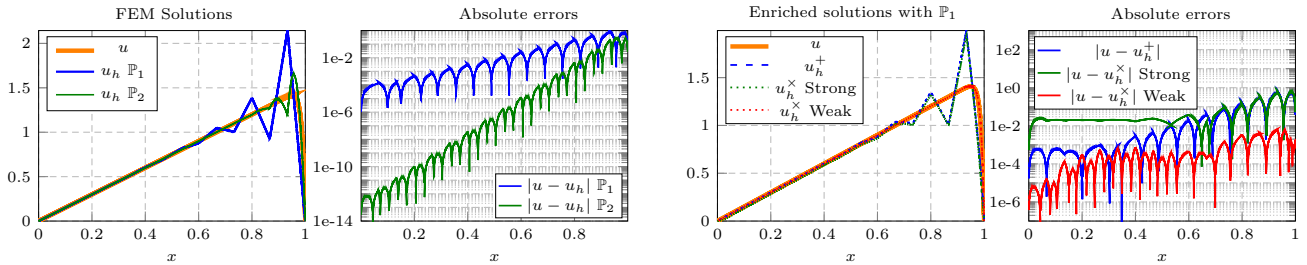


Figure 7: Considering the *1D Elliptic case* with $\mu^{(2)}$ and the PINN prior u_θ , comparison between analytical solution and network prediction. From left to right: solution; first derivative; second derivative; errors.

In Figure 7, we can see that PINN has difficulties to capture the solution and that the prediction it provides is far from the analytical solution. As for its derivatives, they seem to be relatively inaccurate compared to the analytical. Indeed, since the PINN is a smooth function, it has trouble approximating functions with very sharp gradients such as the one of (8.11).

FEM		PINN prior u_θ		
N	error	method	error	gain
16	$1.85 \cdot 10^{-1}$	Add	$1.47 \cdot 10^{-1}$	1.26
32	$6.31 \cdot 10^{-2}$	Add	$5 \cdot 10^{-2}$	1.26
		Mult (strong)	$1.49 \cdot 10^{-1}$	1.24
		Mult (strong)	$6.65 \cdot 10^{-2}$	0.95
		Mult (weak)	$1.6 \cdot 10^{-3}$	115.82
		Mult (weak)	$8.57 \cdot 10^{-4}$	73.7

Table 6: Considering the *1D Elliptic case* with $\mu^{(2)}$, $k = 1$ and $N = 16, 32$. Left – L^2 relative error obtained with FEM. Right – Considering the PINN prior u_θ , L^2 relative errors and gains with respect to FEM, obtained with our methods. Our methods : additive approach, multiplicative approach by taking $M = 0$ (strong and weak BC).



(a) FEM solutions with polynomial order approximation $k = 1$ and $k = 2$, and absolute errors.

(b) Enriched solutions with polynomial order approximation $k = 1$, and absolute errors.

Figure 8: Considering the *1D Elliptic case* with $\mu^{(2)}$, $N = 16$ and the PINN prior u_θ . Comparison of the solution obtained with the different methods with the analytical solution. For each enriched method, comparison of the correction term with the analytical one. Different methods : standard FEM, additive approach, multiplicative approach by taking $M = 0$ (strong and weak BC).

In Figure 8 and Table 6, we present a comparison of the different approaches proposed. In Figure 8a, we first notice the oscillations anticipated in Remark 30 for standard FEM at both polynomial orders $k = 1$ and $k = 2$. This behaviour is also seen in the additive enrichment (blue dashed line in Figure 8b), which does not seem to give better results than standard FEM due to the derivatives presented in Figure 7, and for the multiplicative approach with strong boundary conditions (green dotted line in Figure 8b). However, weakly imposing the BC gives the appropriate results (red dotted line in Figure 8b).

8.3.3 Gains achieved with the additive and the multiplicative approaches

Considering a sample \mathcal{S} of $n_p = 50$ parameters, we will evaluate the gains $G_{+, \theta}$ and G_+ defined in (8.5) with the PINN prior u_θ . We will evaluate $G_{M, \theta}$ and G_M , defined in (8.6), in the same way with $M = 0$ for the multiplicative approach, by considering the two implementations of the boundary conditions; strong and weak BC. The results are presented in Table 7 for fixed $k = 1$ and $N \in \{20, 40\}$ fixed.

method	N	Gains in L^2 rel error of our method w.r.t. PINN				Gains in L^2 rel error of our method w.r.t. FEM			
		min	max	mean	std	min	max	mean	std
Add	20	7.01	93.15	17.97	16.59	1.2	52.18	3.35	6.57
	40	21.19	363.77	68.7	69.83	1.2	46.32	3.29	6.17
Mult (strong)	20	5.29	19.77	9.35	2.51	0.33	13.95	1.58	1.76
	40	10.48	39.89	18.9	4.48	0.16	6.74	0.87	0.84
Mult (weak)	20	69.49	6,247.43	1,479.77	1,094.37	65.32	359.24	186.72	77.12
	40	262.57	24,907.73	4,423.73	3,674.41	54.45	252.57	148.83	48.35

Table 7: Considering the *1D Elliptic case*, $k = 1$ and the PINN prior u_θ . Left – Gains in L^2 relative error of our methods with respect to PINN. Right – Gains in L^2 relative error of our methods with respect to FEM. Our methods : additive approach, multiplicative approach with $M = 0$ (strong and weak BC).

Table 7 confirms the above results. The multiplicative approach with weak BC seems to give the best results on our \mathcal{S} parameter sample. The additive and multiplicative approaches with strong BC imposition do not appear to be very effective on this test case. In particular, even though the additive approach improves the standard FEM error by a factor of 3, we have seen in Section 8.3.2 that the solutions obtained do not correspond to the expected solution, whereas the multiplicative approach with low BCs does. In the following, we will only consider the additive approach, as it seems to be the most efficient one, except in special cases such as the one under consideration in this Section 8.3. Indeed, the following test cases will not contain boundary layers or strong gradients.

8.4 2D Poisson problem in a square domain

We now consider the problem of Section 8.2 but in two dimensions ($d = 2$), with,

$$\begin{cases} -\Delta u = f, & \text{in } \Omega \times \mathcal{M}, \\ u = 0, & \text{on } \partial\Omega \times \mathcal{M}, \end{cases} \quad (8.13)$$

with Δ the Laplace operator on the domain $\Omega = [-0.5\pi, 0.5\pi]^2$ with boundary $\partial\Omega$, and $\mathcal{M} \subset \mathbb{R}^p$ the parameter space (with p the number of parameters). We define the right-hand side f such that the solution is given by

$$u(\mathbf{x}, \boldsymbol{\mu}) = \exp\left(-\frac{(x - \mu_1)^2 + (y - \mu_2)^2}{2}\right) \sin(\kappa x) \sin(\kappa y), \quad (8.14)$$

with $\mathbf{x} = (x, y) \in \Omega$ and some parameters $\boldsymbol{\mu} = (\mu_1, \mu_2) \in \mathcal{M} = [-0.5, 0.5]^p$, hence with $p = 2$ parameters. With an abuse of language as well, we refer to the quantity κ in (8.14) as the frequency of the solution, in the sense that it characterizes the number of oscillations in the solution.

We start with a “low frequency” case in Section 8.4.1, taking $\kappa = 2$ and considering a PINN where we impose the Dirichlet boundary conditions as presented in Section 6.2.1., i.e. using a level-set function. To further improve the prior quality, we introduce an augmented loss function in Section 8.4.2 by using the Sobolev training presented in Section 6.2.2. Afterwards, we test another loss in Section 8.4.3 that includes the Dirichlet condition, or in other words, that does not use a level-set function. Finally, we consider a “higher frequency” case in Section 8.4.4, with $\kappa = 8$.

Remark 32. In the following, the characteristic mesh size $h = \frac{\pi\sqrt{2}}{N-1}$ is defined as a function of N , considering a cartesian mesh of N^2 nodes for our squared 2D domain of length π .

8.4.1 Low-frequency case

We consider a “low-frequency” problem, taking $\kappa = 2$. In this section, we consider the additive approach, as presented in Section 3, by considering the PINN prior u_θ . We start by testing the error estimates in Section 8.4.1.1

(in L^2 norm) with polynomial order $k \in \{1, 2, 3\}$, then we compare the derivatives of the prior and compare the different approaches in [Section 8.4.1.2](#). We evaluate the gains obtained in [Section 8.4.1.3](#) on a sample of parameters. Then, we compare the numerical costs of the different methods in [Section 8.4.1.4](#). Finally we discuss the importance of integrating analytical functions in [Section 8.4.1.5](#), as presented in [Section 7.1](#).

Physics-informed training. Since the problem under consideration is parametric we deploy a parametric PINN, which depends on both the space variable $\mathbf{x} = (x, y) \in \Omega$ and the parameters $\boldsymbol{\mu} = (\mu_1, \mu_2) \in \mathcal{M}$. Moreover, we strongly impose the Dirichlet boundary conditions, as presented in [Section 6.1](#). To do this, we define the prior

$$u_\theta(\mathbf{x}, \boldsymbol{\mu}) = \varphi(\mathbf{x})w_\theta(\mathbf{x}, \boldsymbol{\mu}),$$

where w_θ is the neural network under consideration and φ is a level-set function defined by

$$\varphi(\mathbf{x}) = (x + 0.5\pi)(x - 0.5\pi)(y + 0.5\pi)(y - 0.5\pi),$$

which exactly cancels out on $\partial\Omega$. Since we impose the boundary conditions by using the level-set function, we will only consider the residual loss J_r defined in (6.3) in which the integrals are approached by a Monte-Carlo method, i.e.

$$J_r(\theta) \simeq \frac{1}{N_{\text{col}}} \sum_{i=1}^{N_{\text{col}}} |\Delta u_\theta(\mathbf{x}_{\text{col}}^{(i)}; \boldsymbol{\mu}_{\text{col}}^{(i)}) + f(\mathbf{x}_{\text{col}}^{(i)}; \boldsymbol{\mu}_{\text{col}}^{(i)})|^2$$

with the $N_{\text{col}} = 6000$ collocation points $(\mathbf{x}_{\text{col}}^{(i)}; \boldsymbol{\mu}_{\text{col}}^{(i)})_{i=1, \dots, N_{\text{col}}}$ uniformly chosen on $\Omega \times \mathcal{M}$. Thus, we seek to solve the following minimization problem

$$\theta^* = \underset{\theta}{\operatorname{argmin}} J_r(\theta).$$

The parametric PINN w_θ is defined as an MLP with the hyperparameters defined in [Table 8](#); we use the Adam optimizer and then switch to the LBFGS optimizer after the n_{switch} -th epoch.

Network - MLP		Training - with LBFGS				Loss weights			
<i>layers</i>	40, 60, 60, 60, 40	<i>lr</i>	1.7e-2	<i>n_{epochs}</i>	5000	<i>ω_r</i>	1	<i>ω_{data}</i>	0
<i>σ</i>	sine	<i>decay</i>	0.99	<i>n_{switch}</i>	1000	<i>ω_b</i>	0	<i>ω_{sob}</i>	0
		<i>N_{col}</i>	6000						

Table 8: Network, training parameters ([Remark 13](#)) and loss weights for u_θ in the *2D Laplacian* case.

8.4.1.1 Error estimates

We start by testing the error estimates of [Theorem 6](#) for the following two sets of parameters, randomly selected in \mathcal{M} :

$$\boldsymbol{\mu}^{(1)} = (0.05, 0.22) \quad \text{and} \quad \boldsymbol{\mu}^{(2)} = (0.1, 0.04) \tag{8.15}$$

by considering the PINN prior u_θ . So, for $j \in \{1, 2\}$, the aim is to compare, by varying the mesh size h , the L^2 relative errors $e_h^{(j)}$ obtained with the standard FEM method, defined in (8.1), and $e_{h,+}^{(j)}$ obtained with the additive approach, defined in (8.2). The results are presented in [Figure 9](#) for fixed $k \in \{1, 2, 3\}$ with h depending on $N \in \{16, 32, 64, 128, 256\}$ as presented in [Remark 32](#).

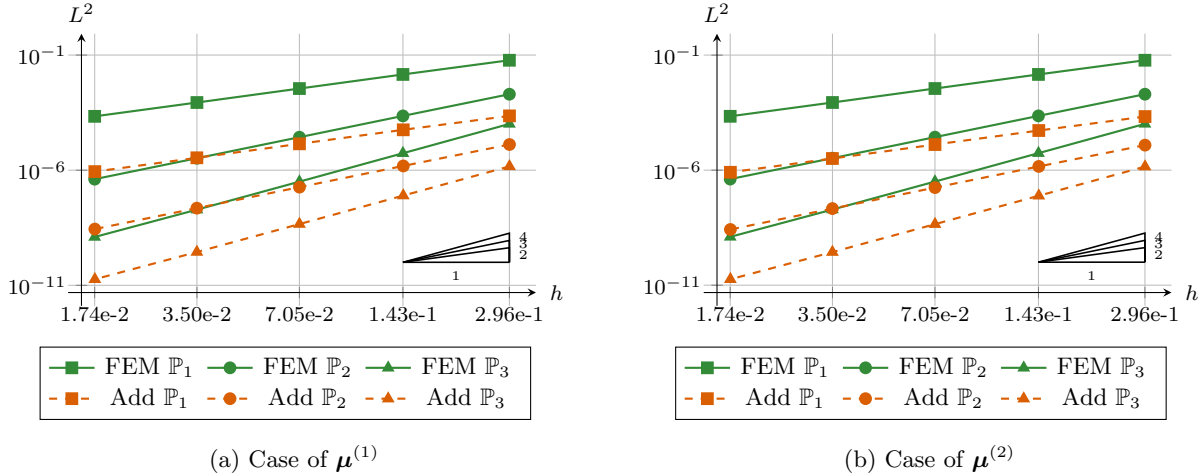


Figure 9: Considering the $2D$ low-frequency case and the PINN prior u_θ . Left – L^2 relative error on h , obtained with the standard FEM $e_h^{(1)}$ (solid lines) and the additive approach $e_{h,+}^{(1)}$ (dashed lines) for $\mu^{(1)}$, with $k \in \{1, 2, 3\}$. Right – Same for $\mu^{(2)}$, (8.15).

In Figure 9, we observe the expected behaviour. Indeed, the error decreases with the correct order of accuracy as the mesh size h decreases. This observation is valid for both the classical and enriched FEM. Moreover, we observe that the error constant of the additive approach is significantly lower than that of the classical FEM. In Section 8.4.1.2, we will compare these different approaches in more detail. As noted in the 1D case, we can see that the additive enriched approach for $k = 1$ (resp. $k = 2$) seems to give the same results as standard FEM for $k = 2$ (resp. $k = 3$).

8.4.1.2 Comparison of different approaches

We now focus on the first parameter $\mu^{(1)}$. We compare the standard FEM method with the additive approach, first in the Table 9 where we can see the different errors obtained with the different methods for $k = 1$ fixed and $N \in \{16, 32\}$ as well as the gains obtained in comparison with standard FEM. Next, we take a closer look at the solution obtained with the different approaches in Figure 10; for each method, we compare the solution obtained (u_h for standard FEM and u_h^+ for the additive approach) with the analytical solution u . For the enriched method, using the PINN prior u_θ , we will also compare the proposed correction; namely, for the additive approach, we will compare p_h^+ with $u - u_\theta$.

FEM		PINN prior u_θ			
N	error	method	N	error	gain
16	$5.95 \cdot 10^{-2}$	Add	16	$2.29 \cdot 10^{-4}$	260.38
32	$1.44 \cdot 10^{-2}$		32	$5.67 \cdot 10^{-5}$	253.66

Table 9: Considering the $2D$ low-frequency case with $\mu^{(1)}$, $k = 1$ and $N \in \{16, 32\}$. Left – L^2 relative error obtained with FEM. Right – Considering the PINN prior u_θ , L^2 relative errors and gains with respect to FEM, obtained with the additive approach.

In Table 9, we observe that the additive approach significantly improves the error of the standard FEM, with gains of around 260 for $N = 16$ and $k = 1$, which is equivalent to refining the mesh by a factor of 16 for \mathbb{P}_1 elements. Indeed, in this case, our enriched approach gives much better results than standard FEM, notably on coarse meshes. In Figure 10, we observe that the solution obtained with the additive approach is very close

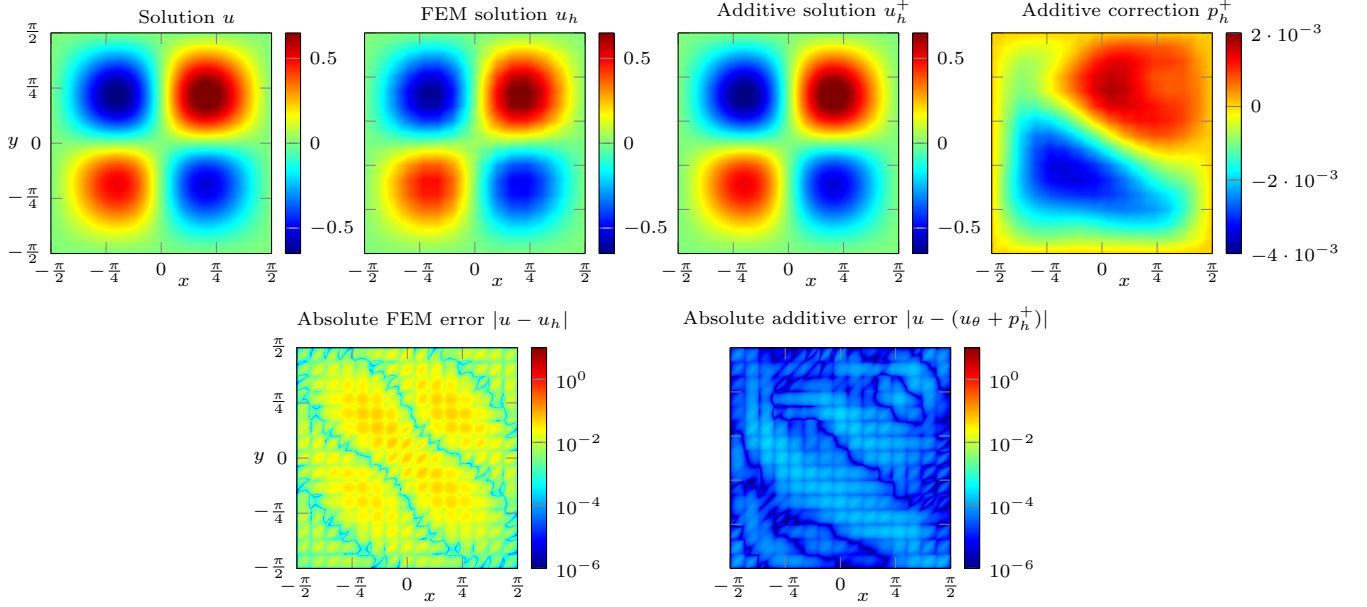


Figure 10: Considering the $2D$ low-frequency case with $\boldsymbol{\mu}^{(1)}$, $k = 1$, $N = 16$ and the PINN prior u_θ . Comparison of the solution obtained with the standard FEM and the additive approach with the analytical solution. For the additive method, comparison of the correction term with the analytical one.

to the analytical solution, with a correction term that is also very close to the analytical one. This shows the effectiveness of the additive approach in this case.

8.4.1.3 Gains achieved with the additive approach

Considering a sample \mathcal{S} of $n_p = 50$ parameters, we now evaluate the gains $G_{+, \theta}$ and G_+ defined in (8.5). The results are presented in Table 10 for $k \in \{1, 2, 3\}$ and $N \in \{20, 40\}$.

k	N	Gains in L^2 rel error of our method w.r.t. PINN				Gains in L^2 rel error of our method w.r.t. FEM			
		min	max	mean	std	min	max	mean	std
1	20	15.69	48.33	33.62	5.56	134.32	377.36	269.39	43.66
	40	61.4	195.53	135.25	23.18	131.2	362.12	262.13	41.68
2	20	244.05	993.21	653.07	153.16	67.02	164.65	134.85	21.29
	40	2,055.16	8,340.94	5,501.88	1,286.49	66.45	159.48	131.86	20.34
3	20	2,780.52	11,705.79	7,542.95	1,766.24	39.52	72.65	61.55	7.02
	40	50,649.24	211,156.91	136,714.04	31,882.69	39.83	72.62	61.67	6.87

Table 10: Considering the $2D$ low-frequency case, $k \in \{1, 2, 3\}$ and the PINN prior u_θ . Left – Gains in L^2 relative error of the additive method with respect to PINN. Right – Gains in L^2 relative error of our approach with respect to FEM.

In Table 10, we observe (left subtable) that our method significantly improves the error of the PINN, especially for large values of k , where the enrichment is performed in a richer approximation space. Moreover, we also observe (right subtable) significant gains with respect to classical FEM. For instance, as expected from the results of Section 8.4.1.2, the mean gains for $k = 1$ are around 270, which corresponds to refining the mesh approximately

16 times for \mathbb{P}_1 elements. This means that our \mathbb{P}_1 enhanced bases capture the solution as accurately as classical \mathbb{P}_1 bases with a mesh four times finer. For $k = 2$ and $k = 3$, the mean gains are around 134 and 61, respectively, which corresponds to refining the mesh approximately 5 times for \mathbb{P}_2 elements and 2.8 times for \mathbb{P}_3 elements. A natural follow-up question consists in assessing the impact of the PINN quality on our results. This will be the subject of the [Section 8.4.2](#).

8.4.1.4 Costs of the different methods

To more accurately assess the benefits of using the enriched methods, we look in this section at the costs of the different methods proposed, considering the parameter $\boldsymbol{\mu}^{(1)}$. Thus, we will consider that the cost of using the PINN prior u_θ , corresponds to the total number of weights of the network considered. In this case, it is given as an MLP with the hyperparameters defined in [Table 8](#), for a total of $N_{\text{weights}} = 12,461$ weights.

For the different finite element methods, we will then try to determine, for a fixed polynomial degree k , the characteristic mesh size h (depending on N as described in [Remark 32](#)) required to reach a fixed error e . In [Table 11](#), we study, for $k \in \{1, 2, 3\}$, considering standard FEM and the additive approach, the N required to achieve the same error e . More precisely, the characteristic mesh size required by standard FEM so that $e_h^{(1)} \approx e$ and the one required by the additive approach so that $e_{h,+}^{(1)} \approx e$. Depending on the polynomial degree k , we can also determine the number of degrees of freedom N_{dofs} associated with each case.

\mathbf{q}	\mathbf{e}	N		N_{dofs}	
		FEM	Add	FEM	Add
1	$1 \cdot 10^{-3}$	119	8	14,161	64
	$1 \cdot 10^{-4}$	379	24	143,641	576
2	$1 \cdot 10^{-4}$	42	8	6,889	225
	$1 \cdot 10^{-5}$	89	17	31,329	1,089
3	$1 \cdot 10^{-5}$	28	10	6,724	784
	$1 \cdot 10^{-6}$	48	18	20,164	2,704

Table 11: Considering the *2D low-frequency* case with $\boldsymbol{\mu}^{(1)}$, $q \in \{1, 2, 3\}$ and the PINN prior u_θ . Left – Characteristic N (associated to the characteristic mesh size h) required to reach a fixed error e for standard FEM and the additive approach. Right – Number of degrees of freedom N_{dofs} associated with each case.

In [Table 11](#), we see that the additive approach proposed in [Section 3](#) requires a much coarser mesh than standard FEM to achieve the same e error. This is due to the error estimations of [Theorem 6](#) which show that the error of the enhanced FEM is significantly lower than that of the classical FEM (depending on the quality of the prior). This is also reflected in the number of degrees of freedom required to achieve the same error e .

Remark 33. *The results in [Table 11](#) have been obtained by interpolating the convergence curves of [Figure 9](#) for the different methods for a given e .*

However, the enriched approaches proposed require using the prior PINN u_θ , which also includes its cost of use. For this reason, it will be interesting to look at these same costs on a set of parameters, say of size $n_p = 100$. Since we are in the context of parametric PINN, we can estimate that the computational cost of solving [\(8.13\)](#) on this sample of n_p parameters corresponds, for the additive approach, to n_p times its number of dofs plus the cost of using PINN (i.e. its total number of weights), thus $n_p \times N_{\text{dofs}} + N_{\text{weights}}$ (with N_{dofs} the number of dofs associated to the additive approach). For standard FEM, this cost is equivalent to n_p times its estimated number of dofs $n_p \times N_{\text{dofs}}$ (with N_{dofs} the number of dofs associated with standard FEM). We will then compare these costs for a set of $n_p = 100$ parameters, considering the same error e to be achieved for both methods. The results are presented in [Table 12](#).

\mathbf{q}	\mathbf{e}	$n_p = 1$		$n_p = 100$	
		FEM	Add	FEM	Add
1	$1 \cdot 10^{-3}$	14,161	12,525	1,416,100	18,861
	$1 \cdot 10^{-4}$	143,641	13,037	14,364,100	70,061
2	$1 \cdot 10^{-4}$	6,889	12,686	688,900	34,961
	$1 \cdot 10^{-5}$	31,329	13,550	3,132,900	121,361
3	$1 \cdot 10^{-5}$	6,724	13,245	672,400	90,861
	$1 \cdot 10^{-6}$	20,164	15,165	2,016,400	282,861

Table 12: Considering the $2D$ low-frequency case, $k \in \{1, 2, 3\}$ and the PINN prior u_θ . Left – Total costs of standard FEM and the additive approach to reach an error e for a set of $n_p = 1$ parameter. Right – Same for a set of $n_p = 100$ parameters.

Remark 34. Note that the Table 12 (right sub-table) is, in fact, only an estimate of the real cost of solving n_p problems. In practice, the number of degrees of freedom N_{dofs} associated with each method depends on the parameter itself. The error to be achieved e will require more or less fine meshes for each parameter.

In Table 12 for $n_p = 1$ (left subtable), we can see that the cost of the additive method is generally lower than that of standard FEM, even though they are of the same range. However, it is important to note that these are not entirely comparable: in fact, a large part of the cost of the additive method lies in PINN prediction, which will be more or less well estimated depending on a number of hyper-parameters (number of epochs, learning rate, etc.). If we then take $n_p = 100$ (right subtable), we can see that the cost of standard FEM becomes radically higher than with the additive approach. This is why the improved approach is particularly interesting for solving the (8.13) problem on a set of parameters.

8.4.1.5 Integration of analytical functions

This section aims to discuss one of the important points, presented in Section 7.1, that enables PINN to be used effectively and can make our enriched methods more or less effective. Indeed, according to (3.3), we have to integrate $f + \Delta u_\theta$ multiplied by the test function. To perform this integration, we first interpolate this term on a polynomial space and then integrate it exactly. The degree of this polynomial approximation is an important parameter to make our technique effective.

The goal here is simply to show that for enriched approaches to be effective, particularly the additive method, this polynomial approximation must be of a sufficiently high degree. Consider the parameter $\mu^{(1)}$, a polynomial degree $k = 3$ and a number of nodes $N = 128$. In Figure 11, we display the L^2 error of the additive approach with respect to the degree of polynomial approximation of $f + \Delta u_\theta$.

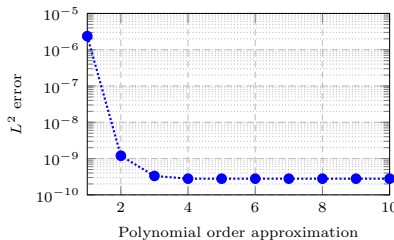


Figure 11: Considering the $2D$ low-frequency case with $\mu^{(1)}$, $q = 3$, $N = 128$ and the PINN prior u_θ . Considering the additive approach, L^2 error $e_{h,+}^{(1)}$ with respect to the degree of polynomial approximation of $f + \Delta u_\theta$.

In Figure 11, we observe that the error decreases as the degree of polynomial approximation increases. This shows the importance of properly interpolating analytical functions in the context of enriched methods.

8.4.2 Low-frequency case — Sobolev training

This section focuses on the same problem as in Section 8.4.1. The aim here is to show that the network quality has a non-negligible impact on the results obtained with our method and that if the network is better, our results will be, too. To this end, we defined a new prior u_θ^{sob} by using the Sobolev training presented in Section 6.2.2, where the derivatives of the solution should be better approximated than by a standard training and compared it with the PINN prior u_θ defined in Section 8.4.1. We start by testing the error estimation in Section 8.4.2.1 with $k \in \{1, 2, 3\}$ polynomial order and evaluate the gains obtained in Section 8.4.2.2 on the same sample of parameters as in Section 8.4.1.

Physics-informed training. We deploy here a parametric PINN, denoted by u_θ^{sob} , where we strongly impose the Dirichlet boundary conditions as in Section 8.4.1. The hyperparameters are defined in Table 13; we use the Adam optimizer and consider N_{col} collocation points, uniformly chosen on Ω .

Remark 35. Adding the Sobolev loss can make training more difficult, so we only consider 3000 epochs but a batch size of 2000. This means that for each epoch, the weights will be updated 3 times (because $N_{\text{col}} = 6000$).

Network - MLP		Training - with LBFGS				Loss weights			
<i>layers</i>	40, 60, 60, 60, 40	<i>lr</i>	1.7e-2	<i>n_{epochs}</i>	3000	<i>ω_r</i>	1	<i>ω_{data}</i>	0
<i>σ</i>	sine	<i>decay</i>	0.99	<i>batch size</i>	2000	<i>ω_b</i>	0	<i>ω_{sob}</i>	0.1
		<i>N_{col}</i>	6000						

Table 13: Network, training parameters (Remark 13) and loss weights for u_θ^{sob} in the 2D Laplacian case.

We consider the residual loss J_r defined in Section 8.4.1 and the Sobolev loss J_{sob} defined in (6.7), whose integrals are both approximated by a Monte-Carlo method. We then seek to solve the following minimisation problem

$$\theta^* = \underset{\theta}{\operatorname{argmin}} \omega_r J_r(\theta) + \omega_{\text{sob}} J_{\text{sob}}(\theta).$$

8.4.2.1 Error estimates

For simplicity, we consider the first parameter $\mu^{(1)} = (0.05, 0.22)$ presented in Section 8.4.1. By varying the mesh size h , we compare the L^2 relative errors between the classical FEM ($e_h^{(1)}$ defined in (8.1)), the enhanced FEM with the prior u_θ from Section 8.4.1, and the enhanced FEM with the current prior u_θ^{sob} ($e_{h,+}^{(1)}$ defined in (8.2)). The results are presented in Figure 12 for fixed $k \in \{1, 2, 3\}$.

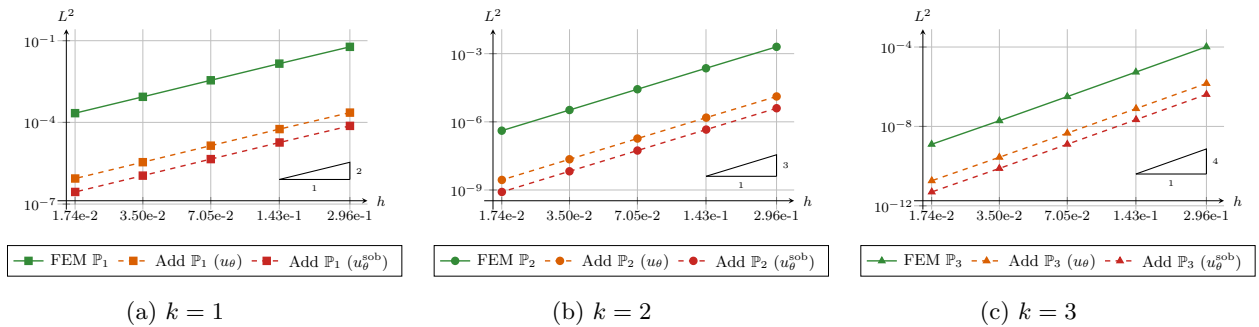


Figure 12: Considering the 2D low-frequency case with $\mu^{(1)}$. Left – L^2 relative error on h , obtained with the standard FEM $e_h^{(1)}$ (solid line) and the additive approach $e_{h,+}^{(1)}$ (dashed lines), with $k = 1$, by considering the PINN prior with standard training u_θ and Sobolev training u_θ^{sob} . Middle – Same with $k = 2$. Right – Same with $k = 3$.

We observe that the Sobolev training improves the results obtained with the L^2 training, for $k \in \{1, 2, 3\}$. This shows the impact of the quality of the network prediction on our method. To further investigate this, we evaluate in [Section 8.4.2.2](#) the gains obtained with the Sobolev training on the same sample of parameters as in [Section 8.4.1](#).

8.4.2.2 Gains achieved with the additive approach

Considering the same sample \mathcal{S} of $n_p = 50$ parameters as in [Section 8.4.1](#), we now evaluate the gains $G_{+, \theta}$ and G_+ defined in (8.5) considering the PINN prior u_θ^{sob} using Sobolev training. The results are presented in [Table 14](#) for $k \in \{1, 2, 3\}$ and $N \in \{20, 40\}$ (with h depending on N as described in [Remark 32](#)).

k	N	Gains in L^2 rel error of our method w.r.t. PINN				Gains in L^2 rel error of our method w.r.t. FEM			
		min	max	mean	std	min	max	mean	std
1	20	16.14	80.38	41.1	15.04	188.69	1,085.32	768.22	200.13
	40	63.93	324.11	166.45	61.46	187.82	1,051.55	751.01	190.72
2	20	263.88	1,751.13	896.03	394.57	147.08	536.32	414.91	78.1
	40	2,235.97	14,849.11	7,600.79	3,349.18	146.35	528.57	408.6	76.94
3	20	3,040.5	22,972.38	10,662.78	5,092.35	91.84	244.09	192.96	32.23
	40	55,299.93	416,438.72	194,157.02	92,537.38	93.16	246.78	194.31	32.51

Table 14: Considering the $2D$ low-frequency case, $k \in \{1, 2, 3\}$ and the PINN prior u_θ^{sob} (Sobolev training). Left – Gains in L^2 relative error of the additive method with respect to PINN. Right – Gains in L^2 relative error of our approach with respect to FEM.

The gains reported in [Table 14](#) show that, compared to L^2 training, Sobolev training increases the mean gains by a factor of about 3. This corresponds to almost half an additional mesh refinement for the \mathbb{P}_1 elements. We also note that this Sobolev training is particularly interesting for higher polynomial degrees, with standard L^2 training having lower gains than for $k = 1$.

8.4.3 Low-frequency case — Boundary loss training

Now, we focus on the same problem as in [Section 8.4.1](#) and [Section 8.4.2](#). We now turn to a standard PINN, denoted by u_θ^{bc} , where we impose the boundary conditions in the loss (no longer with the level-set function). The aim here is to show that our enriched methods also work with priors that do not have exact boundary conditions. To this end, we start by testing the error estimation in [Section 8.4.3.1](#) with $k \in \{1, 2, 3\}$ polynomial order and evaluate the gains obtained in [Section 8.4.3.2](#) on the same sample of parameters as in [Section 8.4.1](#).

Physics-informed training. Since the problem under consideration is parametric, we deploy a parametric PINN and define the prior u_θ^{bc} as an MLP with the hyperparameters defined in [Table 15](#); we use the Adam optimizer and then switch to the LBFGS optimizer after the n_{switch} -th epoch. We consider $N_{\text{col}} = 6000$ collocation points, uniformly chosen on Ω .

Network - MLP		Training - with LBFGS				Loss weights			
<i>layers</i>	40, 60, 60, 60, 40	<i>lr</i>	1.7e-2	<i>n_{epochs}</i>	5000	<i>ω_r</i>	1	<i>ω_{data}</i>	0
<i>σ</i>	sine	<i>decay</i>	0.99	<i>n_{switch}</i>	1000	<i>ω_b</i>	30	<i>ω_{sob}</i>	0
		<i>N_{col}</i>	6000	<i>N_{bc}</i>	2000				

Table 15: Network, training parameters ([Remark 13](#)) and loss weights for u_θ^{bc} in the $2D$ Laplacian case.

We consider the same residual loss as in [Section 8.4.1](#) and the BC loss (where integral are approached by a Monte-Carlo method) is defined by

$$J_b(\theta) \simeq \frac{1}{N_{bc}} \sum_{i=1}^{N_{bc}} |u_\theta^{bc}(\mathbf{x}_{bc}^{(i)}; \boldsymbol{\mu}_{bc}^{(i)})|^2,$$

with $N_{bc} = 2000$ boundary collocation points $(\mathbf{x}_{bc}^{(i)}, \boldsymbol{\mu}_{bc}^{(i)})_{i=1, \dots, N_{bc}}$. Thus we seek to solve the following minimisation problem

$$\theta^* = \underset{\theta}{\operatorname{argmin}} J_r(\theta) + \omega_b J_b(\theta).$$

8.4.3.1 Error estimates

We consider the first parameter $\boldsymbol{\mu}^{(1)} = (0.05, 0.22)$ presented in [Section 8.4.1](#) and by varying the mesh size h , we compare the L^2 relative errors between the classical FEM ($e_h^{(1)}$ defined in (8.1)), the enhanced FEM with the prior u_θ from [Section 8.4.1](#), and the enhanced FEM with the current prior u_θ^{bc} ($e_{h,+}^{(1)}$ defined in (8.2)). The results are presented in [Figure 13](#) for fixed $k \in \{1, 2, 3\}$.

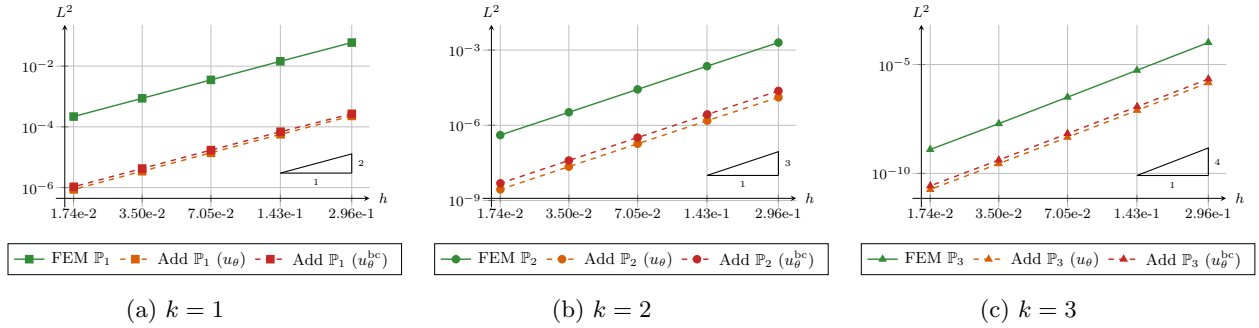


Figure 13: Considering the $2D$ low-frequency case with $\boldsymbol{\mu}^{(1)}$. Left – L^2 relative error on h , obtained with the standard FEM $e_h^{(1)}$ (solid line) and the additive approach $e_{h,+}^{(1)}$ (dashed lines), with $k = 1$, by considering the PINN prior with standard training u_θ and the BC loss training u_θ^{bc} . Middle – Same with $k = 2$. Right – Same with $k = 3$.

We can see in [Figure 13](#) that the additive approach also works when the prior is not exact on the boundary, as here with u_θ^{bc} . In particular, for $k \in \{1, 2, 3\}$ and the parameter $\boldsymbol{\mu}^{(1)}$, our enriched approach using the prior u_θ^{bc} seems to give very similar results to those obtained with u_θ even if the approach with level-set is, for this case, slightly better.

8.4.3.2 Gains achieved with the additive approach

Considering the same sample \mathcal{S} of $n_p = 50$ parameters as in [Section 8.4.1](#), we now evaluate the gains $G_{+,\theta}$ and G_+ defined in (8.5) considering the PINN prior u_θ^{bc} using BC loss training. The results are presented in [Table 16](#) for $k \in \{1, 2, 3\}$ and $N \in \{20, 40\}$.

k	N	Gains in L^2 rel error of our method w.r.t. PINN				Gains in L^2 rel error of our method w.r.t. FEM			
		min	max	mean	std	min	max	mean	std
1	20	21.37	54.17	34.72	6.45	81.13	246.75	168.01	45.92
	40	85.88	220.61	139.04	26.75	80.46	236.88	162.51	43.23
2	20	356.19	1,248.67	579.58	179.56	48.74	91.6	70.04	12.06
	40	3,046.74	10,658.21	4,959.71	1,534.67	48.42	90.91	69.6	11.98
3	20	5,100.32	16,798.35	8,398.62	2,524.2	27.54	52.09	40.41	6.78
	40	92,448.59	308,340.35	152,537.79	46,156.7	27.93	52.21	40.55	6.75

Table 16: Considering the $2D$ low-frequency case, $k \in \{1, 2, 3\}$ and the PINN prior u_θ^{bc} (BC loss training). Left – Gains in L^2 relative error of the additive method with respect to PINN. Right – Gains in L^2 relative error of our approach with respect to FEM.

The gains reported in Table 16 show that for this test case, the use of the prior u_θ (using the level-set) in our enriched approach, seems to give better gains than those of Table 10, considering the current prior u_θ^{bc} . This may be due to the addition of the ω_b^{bc} hyperparameter for balancing losses in training, which may make training less efficient. However, the results obtained with the current prior u_θ^{bc} are still very good, and the gains are still significant compared to the standard FEM.

8.4.4 High-frequency case

To increase in complexity, we investigate a higher-frequency problem by taking $\kappa = 8$ in (8.14). In this section, we start by testing the error estimates in Section 8.4.4.1 with $k \in \{1, 2, 3\}$ polynomial order and evaluate the gains obtained in Section 8.4.4.3 on a sample of parameters.

Physics-informed training. This time, we use the Fourier features from [TS20] as presented in Section 6.2.3 to construct the PINN prior u_θ . The hyperparameters are defined in Table 17; we use the Adam optimizer and then switch to the LBFGS optimizer after the n_{switch} -th epoch. We consider $N_{\text{col}} = 6000$ collocation points, uniformly chosen on Ω . We impose the Dirichlet boundary conditions as in Section 8.4.1 using the level-set function and the same residual loss.

Network - MLP w/ FF		Training - with LBFGS				Loss weights			
<i>layers</i>	40, 60, 60, 60, 40	<i>lr</i>	1.7e-2	<i>n</i> _{epochs}	20000	ω_r	1	ω_{data}	0
σ	sine	<i>decay</i>	0.99	<i>n</i> _{switch}	1000	ω_b	0	ω_{sob}	0
<i>n</i> _f	40	<i>N</i> _{col}	6000						

Table 17: Network, training parameters (Remark 13) and loss weights for u_θ in the $2D$ Laplacian case.

8.4.4.1 Error estimates

We perform the same test as in Section 8.4.1, with a standard training (Sobolev training is not considered).

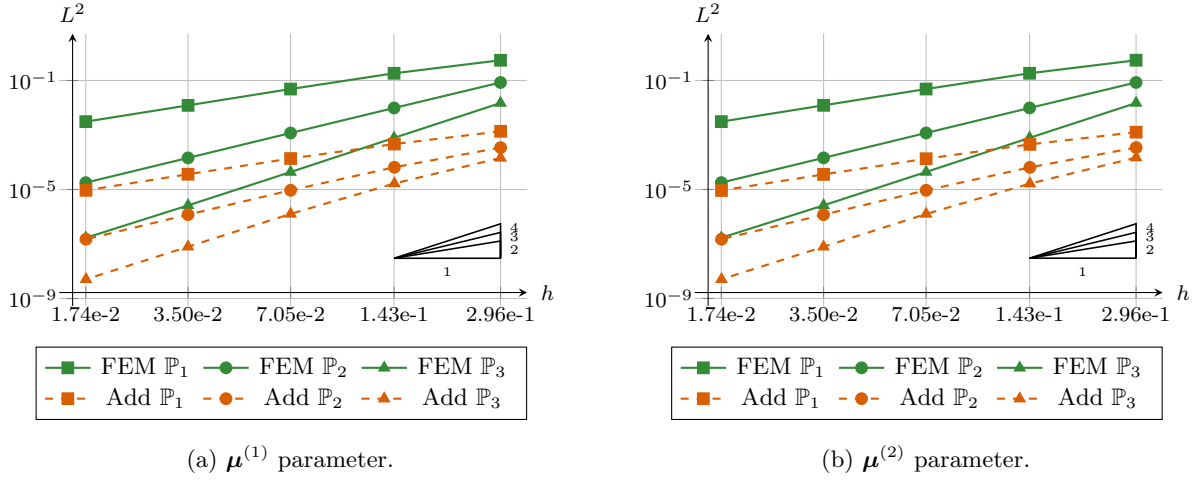


Figure 14: Considering the $2D$ high-frequency case and the PINN prior u_θ . Left – L^2 relative error on h , obtained with the standard FEM $e_h^{(1)}$ (solid lines) and the additive approach $e_{h,+}^{(1)}$ (dashed lines) for $\mu^{(1)}$, with $k \in \{1, 2, 3\}$. Right – Same for $\mu^{(2)}$.

The results displayed in Figure 14, where we observe the expected behavior. Indeed, all schemes have the correct order of accuracy, and the enhanced FEM has a significantly lower error constant than the classical FEM.

8.4.4.2 Comparison of different approaches

We perform the same comparison as in Section 8.4.1.2 for the high-frequency case. We focus on the first parameter $\mu^{(1)}$ and compare the standard FEM method with the additive approach, first in the Table 18 where we can see the different errors obtained with the different methods for $k = 1$ fixed and $N \in \{16, 32\}$ as well as the gains obtained in comparison with standard FEM. Next, we take a closer look at the solution obtained with the different approaches in Figure 15 considering $N = 16$; for each method, we compare the solution obtained (u_h for standard FEM and u_h^+ for the additive approach) with the analytical solution u . For the enriched method, using the PINN prior u_θ , we will also compare the proposed correction; namely, for the additive approach, we will compare p_h^+ with $u - u_\theta$.

FEM		PINN prior u_θ			
N	error	method	N	error	gain
16	$5.53 \cdot 10^{-1}$	Add	16	$1.36 \cdot 10^{-3}$	405.23
32	$1.84 \cdot 10^{-1}$		32	$4.66 \cdot 10^{-4}$	394.18

Table 18: Considering the $2D$ high-frequency case with $\mu^{(1)}$, $k = 1$ and $N = 16, 32$. Left – L^2 relative error obtained with FEM. Right – Considering the PINN prior u_θ , L^2 relative errors and gains with respect to FEM, obtained with the additive approach.

We can see here that the gains obtained in Table 18 are much better than for the “low frequency” case presented in Section 8.4.1. This is, in fact, due to FEM’s difficulty in approximating the solution for high frequencies, especially on coarse meshes. In fact, for the same choice of parameters, the FEM error on this high-frequency problem is 10 times worse than on the low-frequency one, which explains why our gains are so much greater. This also makes the use of the proposed enriched methods particularly interesting. Moreover, we note that while FEM provides a reasonable approximation of the mean of the solution (as evidenced by the second figure on the top row of Figure 15), it is unable to correctly resolve the small-scale oscillating behaviour

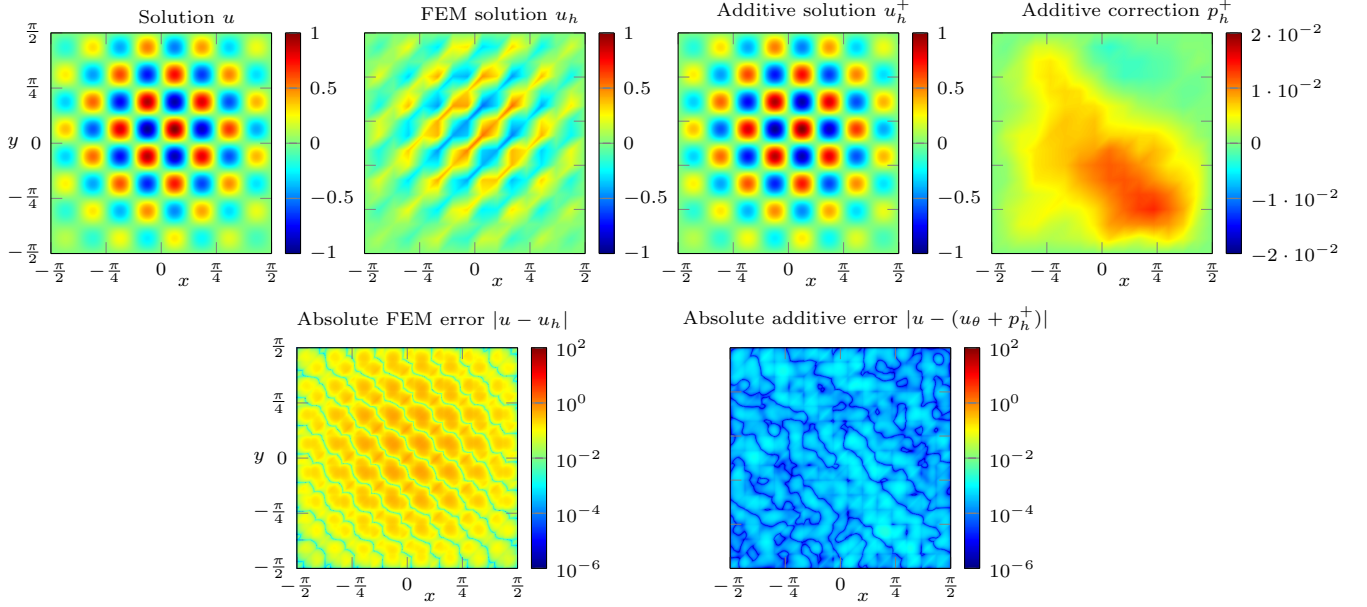


Figure 15: Considering the $2D$ high-frequency case with $\mu^{(1)}$, $k = 1$, $N = 16$ and the PINN prior u_θ . Comparison of the solution obtained with the standard FEM and the additive approach with the analytical solution. For the additive method, comparison of the correction term with the analytical one.

of the solution. The additive correction restores this ability, and the new solution (third figure on the top row of Figure 15) is much better able to capture the oscillations.

8.4.4.3 Gains achieved with the additive approach

We now evaluate the gains $G_{+,\theta}$ and G_+ , defined in (8.5), using the same sample \mathcal{S} of $n_p = 50$ parameters. The results are reported in Table 19 for $k \in \{1, 2, 3\}$ and $N \in \{20, 40\}$.

k	N	Gains in L^2 rel error of our method w.r.t. PINN				Gains in L^2 rel error of our method w.r.t. FEM			
		min	max	mean	std	min	max	mean	std
1	20	9.16	36.18	19.8	6.63	112.19	450.8	349.84	82.9
	40	26.1	111.31	58.78	19.77	106.01	388.91	308.44	71.79
2	20	35.89	164.85	87.44	29.21	65.44	210.59	159.41	38.96
	40	204.25	1,088.02	516.55	179.21	52.5	139.6	109.72	22.04
3	20	100.37	533.16	252.86	88.38	32.91	81.05	63	12.73
	40	971.7	6,165.56	2,592.38	978.71	19.8	41.1	33.53	4.98

Table 19: Considering the $2D$ high-frequency case, $k \in \{1, 2, 3\}$ and the PINN prior u_θ . Left – Gains in L^2 relative error of the additive method with respect to PINN. Right – Gains in L^2 relative error of our approach with respect to FEM.

The same results can be observed in Table 19 as for the $\mu^{(1)}$ parameter. These could be improved by considering a Sobolev training, as in the “low-frequency” case presented in Section 8.4.2.

8.5 2D anisotropic elliptic problem on a square

In this section, we will consider the (1.1) problem in a more complex form than in Section 8.4, by considering the following elliptic problem with homogeneous Dirichlet boundary conditions, in the 2D case ($d = 2$),

$$\begin{cases} -\operatorname{div}(D\nabla u) = f, & \text{in } \Omega, \\ u = 0, & \text{on } \partial\Omega, \end{cases} \quad (8.16)$$

with $\Omega = [0, 1]^2$, $\partial\Omega$ its boundary and $\mathcal{M} \subset \mathbb{R}^p$ the parameter space (with p the number of parameters). Considering $\mathbf{x} = (x, y) \in \Omega$, we define $p = 4$ parameters $\boldsymbol{\mu} = (\mu_1, \mu_2, \epsilon, \sigma) \in \mathcal{M} = [0.4, 0.6] \times [0.4, 0.6] \times [0.01, 1] \times [0.1, 0.8]$. We will then define D , the diffusion matrix (symmetric and positive definite), by

$$D(\mathbf{x}, \boldsymbol{\mu}) = \begin{pmatrix} \epsilon x^2 + y^2 & (\epsilon - 1)xy \\ (\epsilon - 1)xy & x^2 + \epsilon y^2 \end{pmatrix}$$

and the right-hand side f by

$$f(\mathbf{x}, \boldsymbol{\mu}) = \exp\left(-\frac{(x - \mu_1)^2 + (y - \mu_2)^2}{0.025\sigma^2}\right).$$

Note that the matrix D has eigenvalues $x^2 + y^2$ and $\epsilon(x^2 + y^2)$, leading to a diffusion process whose anisotropy increases as ϵ decreases.

Remark 36. In the following, the characteristic mesh size $h = \frac{\sqrt{2}}{N-1}$ is defined as a function of N , considering a Cartesian mesh of N^2 nodes.

Physics-informed training. We then consider a parametric PINN where we exactly impose the Dirichlet boundary conditions as presented in Section 6.2.1. To do this, we define the prior

$$u_\theta(\mathbf{x}, \boldsymbol{\mu}) = \varphi(\mathbf{x})w_\theta(\mathbf{x}, \boldsymbol{\mu}),$$

where w_θ is the neural network under consideration and φ is a level-set function defined by

$$\varphi(\mathbf{x}) = x(x - 1)y(y - 1),$$

which vanishes exactly on $\partial\Omega$. The hyperparameters are defined in Table 20.

Network - MLP		Training		Loss weights			
<i>layers</i>	40, 60, 60, 60, 40	<i>lr</i>	1.6e-2	ω_r	1	ω_{data}	0
σ	tanh	<i>n_{epochs}</i>	15000	ω_b	0	ω_{sob}	0
		<i>N_{col}</i>	8000				

Table 20: Network, training parameters (Remark 13) and loss weights for u_θ in the 2D Elliptic case.

Since we impose the boundary conditions by using the level-set function, we will only consider the residual loss, with integral approached by a Monte-Carlo method, defined by

$$J_r(\theta) \simeq \frac{1}{N_{\text{col}}} \sum_{i=1}^{N_{\text{col}}} |\operatorname{div}(D(\mathbf{x}_{\text{col}}^{(i)}; \boldsymbol{\mu}_{\text{col}}^{(i)}) \nabla u_\theta(\mathbf{x}_{\text{col}}^{(i)}; \boldsymbol{\mu}_{\text{col}}^{(i)})) + f(\mathbf{x}_{\text{col}}^{(i)}; \boldsymbol{\mu}_{\text{col}}^{(i)})|^2,$$

with the $N_{\text{col}} = 8000$ collocation points $(\mathbf{x}_{\text{col}}^{(i)}, \boldsymbol{\mu}_{\text{col}}^{(i)})_{i=1, \dots, N_{\text{col}}}$. Thus we seek to solve the following minimisation problem

$$\theta^* = \operatorname{argmin}_{\theta} J_r(\theta).$$

Remark 37. Here, we do not know the analytical solution associated with the problem under consideration. So, in order to analyze the results obtained, we will define u as a reference solution u_{ref} obtained from a FEM solver on an over-refined mesh of characteristic mesh size h_{ref} and with k_{ref} polynomial order. In this section, we will choose $N_{\text{ref}} = 1000$ (and the associated characteristic mesh size h_{ref} , as defined in Remark 36) and the degree $k_{\text{ref}} = 3$.

8.5.1 Error estimates

We will now test the error estimation (Theorem 6) for the following two sets of parameters, uniformly drawn from \mathcal{M} :

$$\boldsymbol{\mu}^{(1)} = (0.51, 0.54, 0.52, 0.55) \quad \text{and} \quad \boldsymbol{\mu}^{(2)} = (0.48, 0.53, 0.41, 0.89).$$

So, for $j \in \{1, 2\}$, the aim is to compare, by varying the mesh size h , the L^2 relative errors $e_h^{(j)}$ obtained with the standard FEM method, defined in (8.1), and $e_{h,+}^{(j)}$ obtained with the additive approach, defined in (8.2). The results are presented in Figure 16 for a fixed $k \in \{1, 2, 3\}$ with $N \in \{16, 32, 64, 128, 256\}$, as presented in Remark 36.

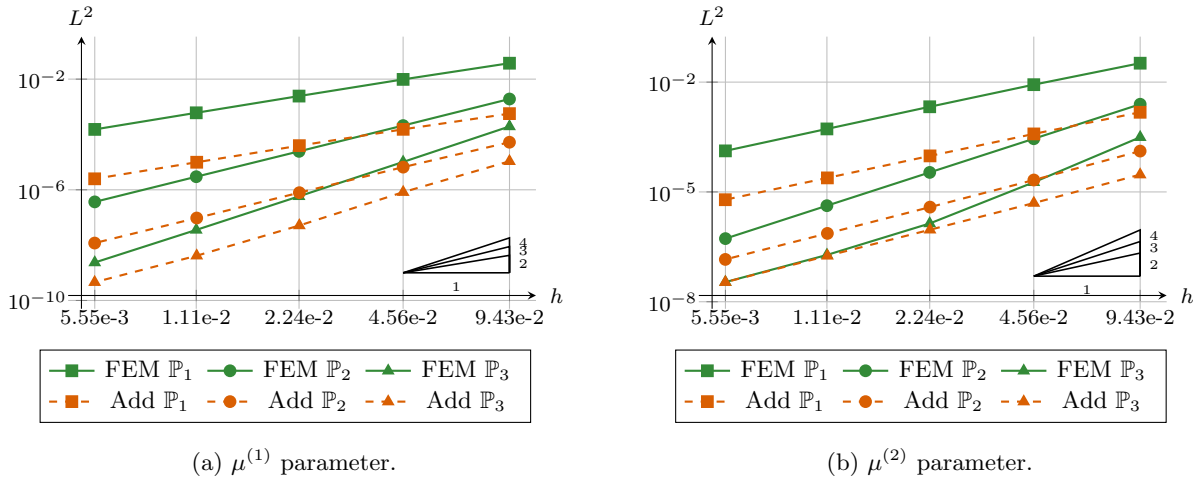


Figure 16: Considering the $2D$ elliptic case and the PINN prior u_θ . Left – L^2 relative error on h , obtained with the standard FEM $e_h^{(1)}$ (solid lines) and the additive approach $e_{h,+}^{(1)}$ (dashed lines) for $\boldsymbol{\mu}^{(1)}$, with $k \in \{1, 2, 3\}$. Right – Same for $\boldsymbol{\mu}^{(2)}$.

As in the other test cases, the two approaches tested appear to respect the correct slopes of Theorem 5 and Theorem 6. The additive approach seems to be more efficient than the standard FEM method for polynomial orders $k \in \{1, 2, 3\}$ and for the two sets of parameters considered.

8.5.2 Comparison of different approaches

We perform the same comparison as in Section 8.4.1.2 for this elliptic case. We focus on the first parameter $\boldsymbol{\mu}^{(1)}$ by taking a closer look at the solution obtained with the different approaches in Figure 17 considering $N = 16$ and $k = 2$; for each method, we compare the solution obtained (u_h for standard FEM and u_h^+ for the additive approach) with the analytical solution u . For the enriched method, using the PINN prior u_θ , we will also compare the proposed correction; namely, for the additive approach, we will compare p_h^+ with $u - u_\theta$.

We observe that the enriched FEM provides a more accurate solution compared to the standard FEM one. The results indicate that the additive approach is particularly effective in capturing the solution's finer details. This demonstrates its potential in solving anisotropic problems with higher accuracy than standard methods.

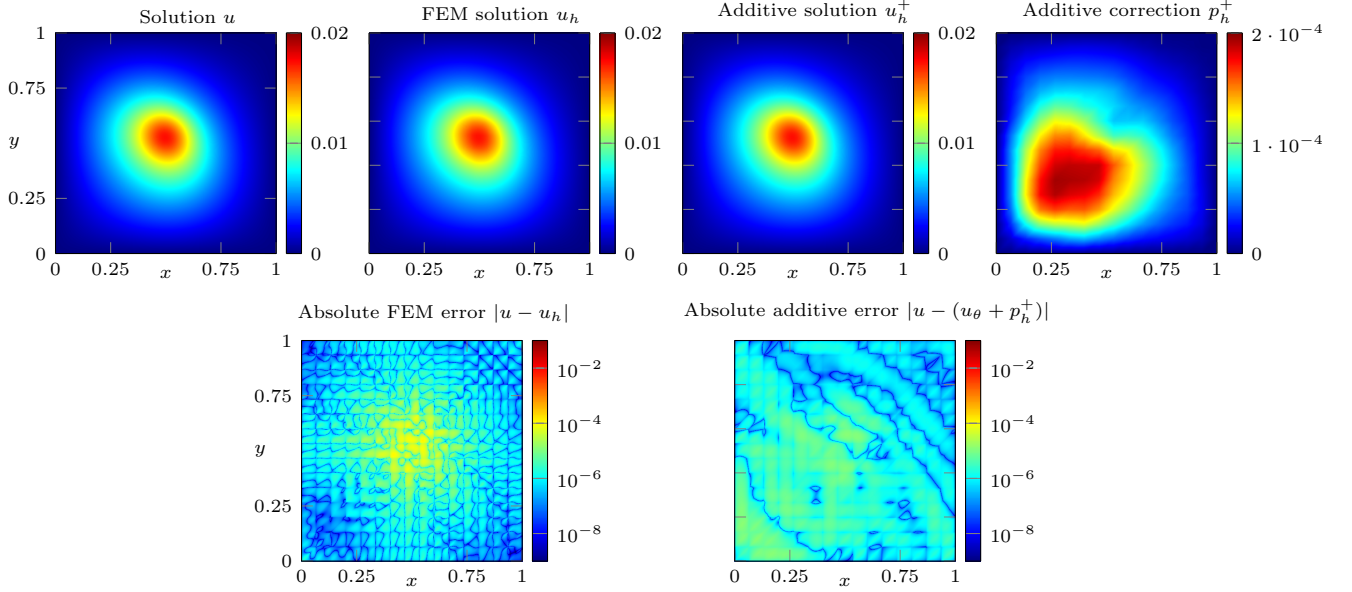


Figure 17: Considering the $2D$ elliptic case with $\mu^{(1)}$, $k = 2$, $N = 16$ and the PINN prior u_θ . Comparison of the solution obtained with the standard FEM and the additive approach with the analytical solution. For the additive method, comparison of the correction term with the analytical one.

8.5.3 Gains achieved with the additive approach

Considering a sample \mathcal{S} of $n_p = 50$ parameters, we will evaluate the gains $G_{+, \theta}$ and G_+ defined in (8.5). The results are presented in Table 21 for $k \in \{1, 2, 3\}$ fixed and $N \in \{20, 40\}$ fixed.

k	N	Gains in L^2 rel error of our method w.r.t. PINN				Gains in L^2 rel error of our method w.r.t. FEM			
		min	max	mean	std	min	max	mean	std
1	20	2.26	50.1	17.35	11.21	7.12	82.57	35.67	17.55
	40	4.84	185.73	62.52	43.15	6.8	77.55	33.91	16.36
2	20	15.03	623.17	213.18	143.68	3.54	35.88	18.32	7.95
	40	118.35	4,942.28	1,560	1,096.15	2.37	31.82	14.83	7.49
3	20	151.67	3,295.53	1,111.11	750.19	1.33	26.51	8.32	5.02
	40	1,939.42	62,146.51	14,375.23	12,088.42	1.03	19.8	5.77	3.86

Table 21: Considering the $2D$ elliptic case, $k \in \{1, 2, 3\}$ and the PINN prior u_θ . Left – Gains in L^2 relative error of the additive method with respect to PINN. Right – Gains in L^2 relative error of our approach with respect to FEM.

As in the previous test cases, the additive approach seems to be more efficient than the standard FEM method for the two polynomial orders $k \in \{1, 2, 3\}$ and for the two mesh sizes $N \in \{20, 40\}$. However, the gains obtained are less significant than in the previous test cases. This is due to the fact that the problem under consideration is more complex, and thus, the prior u_θ is less accurate.

8.6 2D Poisson problem on an annulus, with mixed boundary conditions

This section concerns the problem (1.1), considering the Poisson problem with mixed (Dirichlet and Robin) boundary conditions defined in two space dimensions ($d = 2$) by

$$\begin{cases} -\Delta u = f, & \text{in } \Omega \times \mathcal{M}, \\ u = g, & \text{on } \Gamma_E \times \mathcal{M}, \\ \frac{\partial u}{\partial n} + u = g_R, & \text{on } \Gamma_I \times \mathcal{M}, \end{cases}$$

with $\mathcal{M} \subset \mathbb{R}^p$ the parameter space (with p the number of parameters). We consider Ω to be an annulus, defined by the unit circle (circle of radius 1 and centre $(0, 0)$) with a circular hole (of radius 0.25 and centre $(0, 0)$). We then define $\partial\Omega = \Gamma_I \cup \Gamma_E$ the boundary of Ω , with Γ_I the inner boundary (the hole) and Γ_E the outer boundary (the unit circle). We consider the analytical solution defined for all $\mathbf{x} = (x, y) \in \Omega$ by

$$u(\mathbf{x}; \boldsymbol{\mu}) = 1 - \frac{\ln(\mu_1 \sqrt{x^2 + y^2})}{\ln(4)},$$

with some parameters $\boldsymbol{\mu} = \mu_1 \in [2.4, 2.6]$ ($p = 1$ parameter), and the associated right-hand side $f = 0$. The Dirichlet condition g on Γ_E is also defined by

$$g(\mathbf{x}; \boldsymbol{\mu}) = 1 - \frac{\ln(\mu_1)}{\ln(4)}$$

and the Robin condition g_R on Γ_I is defined by

$$g_R(\mathbf{x}; \boldsymbol{\mu}) = 2 + \frac{4 - \ln(\mu_1)}{\ln(4)}.$$

In this section, we consider the additive approach, as presented in Section 3, by considering the PINN prior u_θ . We start by testing the error estimation in Section 8.6.1 with $k \in \{1, 2, 3\}$ polynomial order and evaluate the gains obtained in Section 8.6.3 on a sample of parameters.

Remark 38. *To avoid geometric errors, we apply Remark 25, by considering that $g = u$ on $\Gamma_{E,h}$ and $g_R = \frac{\partial u}{\partial n}$ on $\Gamma_{I,h}$, with $\Gamma_{E,h}$ and $\Gamma_{I,h}$ the respective outer and inner boundaries of Ω_h , the domain covered by the mesh. Note also that u_θ is not exact on these approximate boundaries.*

Physics-informed training. Since the problem under consideration is parametric, we deploy a parametric PINN, which depends on both the space variable $\mathbf{x} = (x, y) \in \Omega$ and the parameters $\boldsymbol{\mu} = \mu_1 \in \mathcal{M}$. To improve the derivatives' quality, we consider the Sobolev training presented in Section 6.2.2. Moreover, we strongly impose the Dirichlet boundary conditions, as explained in Section 6.2.1, by using the formulation proposed in [SS22]. To do this, we define the prior

$$u_\theta = \frac{\varphi_E}{\varphi_E + \varphi_I^2} [w_\theta + \varphi_I (w_\theta - \nabla \varphi_I \cdot \nabla w_\theta - h)] + \frac{\varphi_I^2}{\varphi_E + \varphi_I^2} g + \varphi_E \varphi_I^2 w_\theta, \quad (8.17)$$

where w_θ is the neural network under consideration and φ_I and φ_E are respectively the signed distance functions to Γ_I and Γ_E defined by

$$\varphi_I(\mathbf{x}) = \sqrt{x^2 + y^2} - 0.25, \quad \varphi_E(\mathbf{x}) = 1 - \sqrt{x^2 + y^2},$$

which cancels out exactly on Γ_I and Γ_E .

In this case, we consider an MLP with 5 layers and a tanh activation function with the hyperparameters defined in Table 22; we use the Adam optimizer [KB15] and consider $N_{\text{col}} = 6000$ collocation points, uniformly chosen on Ω .

Remark 39. *Note that the level sets considered are signed distance functions in this specific test case, which is not the case in the other test cases. In this test case, this is necessary because of the formulation proposed in (8.17) by [SS22].*

Network - MLP		Training - with LBFGS				Loss weights			
<i>layers</i>	40, 40, 40, 40, 40	<i>lr</i>	1e-2	<i>n_epochs</i>	4000	ω_r	1	ω_{data}	0
σ	tanh	<i>decay</i>	0.99	<i>n_switch</i>	3000	ω_b	0	ω_{sob}	0
		<i>N_{col}</i>	6000						

Table 22: Network, training parameters (Remark 13) and loss weights for u_θ in the $2D$ Laplacian case on an Annulus.

Since we impose the boundary conditions by using the level-set function, we will only consider the residual loss, where the integral is approached by a Monte-Carlo method, defined by

$$J_r(\theta) \simeq \frac{1}{N_{\text{col}}} \sum_{i=1}^{N_{\text{col}}} |\Delta u_\theta(\mathbf{x}_{\text{col}}^{(i)}; \boldsymbol{\mu}_{\text{col}}^{(i)}) + f(\mathbf{x}_{\text{col}}^{(i)}; \boldsymbol{\mu}_{\text{col}}^{(i)})|^2,$$

with the N_{col} collocation points $(\mathbf{x}_{\text{col}}^{(i)}, \boldsymbol{\mu}_{\text{col}}^{(i)})_{i=1, \dots, N_{\text{col}}}$. Considering the Sobolev training, we seek to solve the following minimisation problem

$$\theta^* = \omega_r \underset{\theta}{\operatorname{argmin}} J_r(\theta) + \omega_{\text{sob}} J_{\text{sob}}(\theta),$$

with $\omega_r = 1$ and $\omega_{\text{sob}} = 0.1$ the weights associated with the residual and Sobolev losses, respectively.

8.6.1 Error estimates

We start by testing the error estimation of Theorem 6 for the following two sets of parameters, uniformly selected from \mathcal{M} :

$$\boldsymbol{\mu}^{(1)} = (2.51) \quad \text{and} \quad \boldsymbol{\mu}^{(2)} = (2.54)$$

by considering the PINN prior u_θ . So, for $j \in \{1, 2\}$, the aim is to compare, by varying the mesh size h , the L^2 relative errors $e_h^{(j)}$ obtained with the standard FEM method, defined in (8.1), and $e_{h,+}^{(j)}$ obtained with the additive approach, defined in (8.2). The results are presented in Figure 9 for fixed $k \in \{1, 2, 3\}$ by varying the mesh size h .

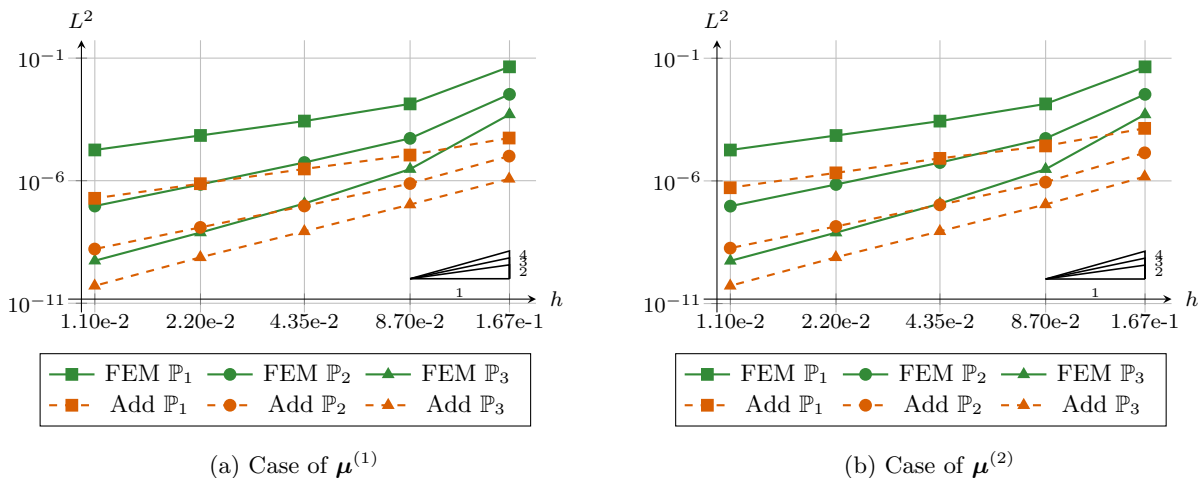


Figure 18: Considering the $2D$ Laplacian case on an Annulus and the PINN prior u_θ . Left – L^2 relative error on h , obtained with the standard FEM $e_h^{(1)}$ (solid lines) and the additive approach $e_{h,+}^{(1)}$ (dashed lines) for $\boldsymbol{\mu}^{(1)}$, with $k \in \{1, 2, 3\}$. Right – Same for $\boldsymbol{\mu}^{(2)}$.

As expected, we see in [Figure 18](#) that the error estimates are confirmed by the numerical results obtained with the standard FEM and the additive approach. The error decreases with the correct order of convergence for these two methods. Furthermore, the enriched approach provides a better accuracy than the standard FEM, as expected.

8.6.2 Comparison of different approaches

We perform the same comparison as in [Section 8.4.1.2](#) for this elliptic case. We focus on the first parameter $\mu^{(1)}$ by taking a closer look at the solution obtained with the different approaches in [Figure 19](#) considering $h \simeq 1.67 \cdot 10^{-1}$ and $k = 1$; for each method, we compare the solution obtained (u_h for standard FEM and u_h^+ for the additive approach) with the analytical solution u . For the enriched method, using the PINN prior u_θ , we will also compare the proposed correction; namely, for the additive approach, we will compare p_h^+ with $u - u_\theta$.

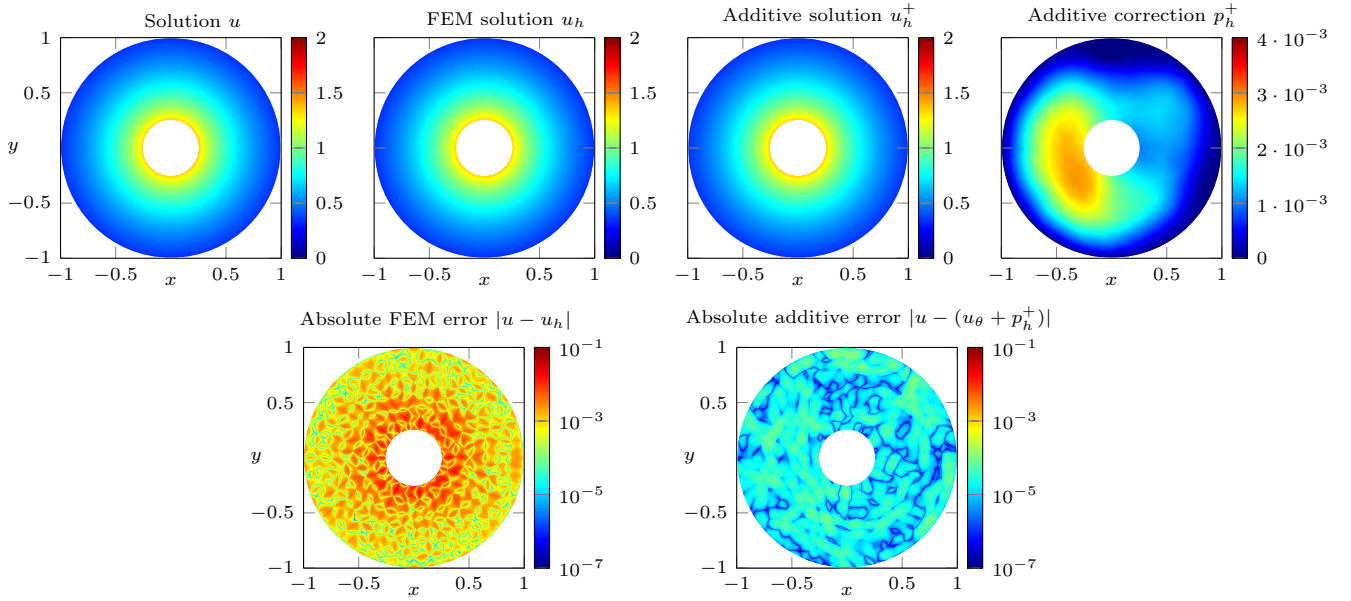


Figure 19: Considering the *2D Laplacian* case on an Annulus with $\mu^{(1)}$, $k = 1$, $h \simeq 1.67 \cdot 10^{-1}$ and the PINN prior u_θ . Comparison of the solution obtained with the standard FEM and the additive approach with the analytical solution. For the additive method, comparison of the correction term with the analytical one.

Once again, we observe that the enriched approach provides a significant improvement in accuracy compared to the standard FEM. This demonstrates the effectiveness of incorporating neural network priors in the case of mixed boundary conditions on more complex geometries than squares (here, on an annulus).

8.6.3 Gains achieved with the additive approach

Considering a sample \mathcal{S} of $n_p = 50$ parameters, we now evaluate the gains $G_{+, \theta}$ and G_+ defined in [\(8.5\)](#). The results are presented in [Table 23](#) for $k \in \{1, 2, 3\}$ and $h \in \{1.33 \cdot 10^{-1}, 6.90 \cdot 10^{-2}\}$.

k	h	Gains in L^2 rel error of our method w.r.t. PINN				Gains in L^2 rel error of our method w.r.t. FEM			
		min	max	mean	std	min	max	mean	std
1	$1.33 \cdot 10^{-1}$	51.44	154.48	124.76	31.45	15.12	137.72	55.5	38.24
	$6.9 \cdot 10^{-2}$	186.44	569.39	460.53	118.34	14.35	124.91	51.72	34.68
2	$1.33 \cdot 10^{-1}$	551.64	5,688.06	3,401.69	1,674.34	31	77.46	58.41	15.46
	$6.9 \cdot 10^{-2}$	3,148.05	39,267.58	21,619.73	11,644.3	28.45	58.98	47.17	10.1
3	$1.33 \cdot 10^{-1}$	2,005.65	51,857	19,839.47	14,735.78	18.72	21.49	20.6	0.82
	$6.9 \cdot 10^{-2}$	29,270.47	681,417.4	281,187.12	197,765.09	17.92	19.85	19.33	0.57

Table 23: Considering the $2D$ Laplacian case on an Annulus, $k \in \{1, 2, 3\}$ and the PINN prior u_θ . Left – Gains in L^2 relative error of the additive method with respect to PINN. Right – Gains in L^2 relative error of our approach with respect to FEM.

As in previous sections, the PINN-enriched approach seems to give better results than standard FEM. For $k = 1$ we see a gain of 50 on average for this test case, which is equivalent to refining the mesh by a factor of 7 for \mathbb{P}_1 elements.

9 Conclusion and future works

In this work, we explored a new approach combining FEM and predictions from neural networks. The FEM scheme is used to enhance the prediction thanks to a correction. Two strategies were investigated: an additive correction and a multiplicative one. For both approaches, we have proved a priori error estimates for both the H^1 semi-norm and the L^2 norm. We have also highlighted a link between these two techniques. Moreover, the constant appearing in these inequalities is compared with the case of classical FEM. Numerical simulations on parametric problems in one and two dimensions confirm our theoretical analyses. The various numerical test cases have shown that PINNs are good candidates for our enriched methods due to their ability to approximate the derivatives of the solution, which is necessary for the quality of our techniques. Their ability to approximate the solution of the parametric PDE over a set of parameters also showed that the proposed approaches are much more interesting in terms of numerical costs than the standard method. Solutions to improve the quality of the prior and, thus, the quality of the results have also been highlighted, with Sobolev training in particular. We have also observed that the additive approach offers greater robustness and a more straightforward implementation than the multiplicative one.

The present work opens up several perspectives. For instance, the additive and multiplicative can be easily adapted to non-linear equations. Moreover, the prediction could also be used to build an optimal mesh before the FEM resolution, for instance, via a posteriori error estimates.

10 Acknowledgment

This work was supported by the Agence Nationale de la Recherche, Project PhiFEM, under grant ANR-22-CE46-0003-01.

References

- [AS97] R. C. Almeida and R. S. Silva. A stable Petrov-Galerkin method for convection-dominated problems. *Comput. Method. Appl. M.*, 140(3–4):291–304, 1997.
- [BMP⁺19] J.-N. Brunet, A. Mendizabal, A. Petit, N. Golse, É. Vibert, and S. Cotin. Physics-based deep neural network for augmented reality during liver surgery. In *Medical Image Computing and Computer Assisted Intervention – MICCAI 2019*, pages 137–145. Springer International Publishing, 2019.

- [BS08] S. C. Brenner and L. R. Scott. *The Mathematical Theory of Finite Element Methods*. Springer New York, 2008.
- [Caf98] R. E. Caflisch. Monte Carlo and quasi-Monte Carlo methods. *Acta Numer.*, 7:1–49, 1998.
- [CDCG⁺22] S. Cuomo, V. S. Di Cola, F. Giampaolo, G. Rozza, M. Raissi, and F. Piccialli. Scientific Machine Learning Through Physics-Informed Neural Networks: Where we are and What’s Next. *J. Sci. Comput.*, 92(3), 2022.
- [CDG08] B. Cockburn, B. Dong, and J. Guzmán. A superconvergent LDG-hybridizable Galerkin method for second-order elliptic problems. *Math. Comput.*, 77(264):1887–1916, 2008.
- [CDL⁺23] S. Cotin, M. Duprez, V. Lleras, A. Lozinski, and K. Vuillemot. ϕ -FEM: An Efficient Simulation Tool Using Simple Meshes for Problems in Structure Mechanics and Heat Transfer. In *Partition of Unity Methods*, pages 191–216. Wiley Online Library, 2023.
- [Cia02] P. G. Ciarlet. *The Finite Element Method for Elliptic Problems*. Society for Industrial and Applied Mathematics, 2002.
- [Dem23] L. F. Demkowicz. *Mathematical Theory of Finite Elements*. Society for Industrial and Applied Mathematics, 2023.
- [DHMM24] V. Dolean, A. Heinlein, S. Mishra, and B. Moseley. Multilevel domain decomposition-based architectures for physics-informed neural networks. *Comput. Method. Appl. M.*, 429:117116, 2024.
- [DL20] M. Duprez and A. Lozinski. ϕ -FEM: A Finite Element Method on Domains Defined by Level-Sets. *SIAM J. Numer. Anal.*, 58(2):1008–1028, 2020.
- [DLL22] M. Duprez, V. Lleras, and A. Lozinski. A new ϕ -FEM approach for problems with natural boundary conditions. *Numer. Meth. Part. D. E.*, 39(1):281–303, 2022.
- [DLL23] M. Duprez, V. Lleras, and A. Lozinski. ϕ -FEM: an optimally convergent and easily implementable immersed boundary method for particulate flows and Stokes equations. *ESAIM: Mathematical Modelling and Numerical Analysis*, 57(3):1111–1142, 2023.
- [DLLV23] M. Duprez, V. Lleras, A. Lozinski, and K. Vuillemot. ϕ -FEM for the heat equation: optimal convergence on unfitted meshes in space. *C. R. Math.*, 361(G11):1699–1710, 2023.
- [EG04] A. Ern and J.-L. Guermond. *Theory and Practice of Finite Elements*. Springer New York, 2004.
- [Eva22] L. C. Evans. *Partial differential equations*. Number 19 in Graduate studies in mathematics. American Mathematical Society, Providence, Rhode Island, second edition, 2022.
- [EY18] W. E and B. Yu. The Deep Ritz Method: A Deep Learning-Based Numerical Algorithm for Solving Variational Problems. *Commun. Math. Stat.*, 6(1):1–12, 2018.
- [FBCD22] Stefano Frambati, Hélène Barucq, Henri Calandra, and Julien Diaz. Practical unstructured splines: Algorithms, multi-patch spline spaces, and some applications to numerical analysis. *Journal of Computational Physics*, 471:111625, 2022.
- [FMDN24] E. Franck, V. Michel-Dansac, and L. Navoret. Approximately well-balanced Discontinuous Galerkin methods using bases enriched with Physics-Informed Neural Networks. *J. Comput. Phys.*, 512:113144, 2024.
- [FST⁺24] X. Feng, H. Shanguan, T. Tang, X. Wan, and T. Zhou. A hybrid FEM-PINN method for time-dependent partial differential equations, 2024. arXiv:2409.02810 [math].
- [GKLS24] T. G. Grossmann, U. J. Komorowska, J. Latz, and C.-B. Schönlieb. Can physics-informed neural networks beat the finite element method? *IMA J. Appl. Math.*, 89(1):143–174, 2024.

- [HCB05] Thomas JR Hughes, John A Cottrell, and Yuri Bazilevs. Isogeometric analysis: Cad, finite elements, nurbs, exact geometry and mesh refinement. *Computer methods in applied mechanics and engineering*, 194(39-41):4135–4195, 2005.
- [HMP13] Ralf Hiptmair, Andrea Moiola, and Ilaria Perugia. Error analysis of trefftz-discontinuous galerkin methods for the time-harmonic maxwell equations. *Mathematics of Computation*, 82(281):247–268, 2013.
- [HPS17] A. Hungria, D. Prada, and F.-J. Sayas. HDG methods for elastodynamics. *Comput. Math. Appl.*, 74(11):2671–2690, 2017.
- [IGMS22] L.-M. Imbert-Gérard, A. Moiola, and P. Stocker. A space-time quasi-Trefftz DG method for the wave equation with piecewise-smooth coefficients. *Math. Comp.*, 92(341):1211–1249, 2022.
- [JKN18] V. John, P. Knobloch, and J. Novo. Finite elements for scalar convection-dominated equations and incompressible flow problems: a never ending story? *Comput. Vis. Sci.*, 19(5–6):47–63, 2018.
- [KB15] D. Kingma and J. Ba. Adam: A Method for Stochastic Optimization. In *International Conference on Learning Representations (ICLR)*, San Diego, CA, USA, 2015.
- [KZK21] E. Kharazmi, Z. Zhang, and G. E. M. Karniadakis. hp-VPINNs: Variational physics-informed neural networks with domain decomposition. *Comput. Methods Appl. Mech. Engrg.*, 374:113547, 2021.
- [LLF98] I. E. Lagaris, A. Likas, and D. I. Fotiadis. Artificial neural networks for solving ordinary and partial differential equations. *IEEE Trans. Neural Netw.*, 9(5):987–1000, 1998.
- [MP18] Andrea Moiola and Ilaria Perugia. A space-time trefftz discontinuous galerkin method for the acoustic wave equation in first-order formulation. *Numerische Mathematik*, 138(2):389–435, 2018.
- [Pea19] A. Paszke and S. Gross et al. *PyTorch: an imperative style, high-performance deep learning library*, pages 8026–8037. Curran Associates Inc., Red Hook, NY, USA, 2019.
- [PFB24] H. Pham, F. Faucher, and H. Barucq. Numerical investigation of stabilization in the Hybridizable Discontinuous Galerkin method for linear anisotropic elastic equation. *Comput. Method. Appl. M.*, 428:117080, 2024.
- [PFS+19] J. J. Park, P. Florence, J. Straub, R. Newcombe, and S. Lovegrove. DeepSDF: Learning Continuous Signed Distance Functions for Shape Representation. In *2019 IEEE/CVF Conference on Computer Vision and Pattern Recognition (CVPR)*, pages 165–174. IEEE, 2019.
- [Red19] J. N. Reddy. *Introduction to the Finite Element Method, Fourth Edition*. McGraw-Hill Education, New York, N.Y., 4th edition. edition, 2019. Includes bibliographical references and index. - Description based on e-Publication PDF.
- [RPK19] M. Raissi, P. Perdikaris, and G. E. Karniadakis. Physics-informed neural networks: A deep learning framework for solving forward and inverse problems involving nonlinear partial differential equations. *J. Comput. Phys.*, 378:686–707, 2019.
- [SDSG24] K. Skardova, A. Daby-Seesaram, and M. Genet. Finite Element Neural Network Interpolation. Part I: Interpretable and Adaptive Discretization for Solving PDEs, December 2024. arXiv:2412.05719 [math].
- [SJHH21] H. Son, J. W. Jang, W. J. Han, and H. J. Hwang. Sobolev training for physics informed neural networks, 2021.
- [SKPP24] M. Sikora, P. Krukowski, A. Paszyńska, and M. Paszyński. Comparison of Physics Informed Neural Networks and Finite Element Method Solvers for advection-dominated diffusion problems. *J. Comput. Sci.*, 81:102340, 2024.

- [SMB⁺20] V. Sitzmann, J. Martel, A. Bergman, D. Lindell, and G. Wetzstein. Implicit neural representations with periodic activation functions. In H. Larochelle, M. Ranzato, R. Hadsell, M.F. Balcan, and H. Lin, editors, *Advances in Neural Information Processing Systems*, volume 33, pages 7462–7473. Curran Associates, Inc., 2020.
- [SS22] N. Sukumar and A. Srivastava. Exact imposition of boundary conditions with distance functions in physics-informed deep neural networks. *Comput. Method. Appl. M.*, 389:114333, 2022.
- [SY06] W. Sun and Y.-X. Yuan. Quasi-Newton Methods. In *Numerical Optimization*, New York, NY, 2006. Springer.
- [TS20] M. Tancik and P. et al. Srinivasan. Fourier Features Let Networks Learn High Frequency Functions in Low Dimensional Domains. In *Advances in Neural Information Processing Systems*, volume 33, pages 7537–7547. Curran Associates, Inc., 2020.

A Notations and definitions

The aim of this section is to introduce the notations used throughout the paper. We first present the notations related to the parametric PDE (Table 24), to the neural network (Table 25), and to the finite element methods (Table 26).

Notation	Definition
Ω	Spatial domain
d	Spatial dimension
$\mathbf{x} = (x_1, \dots, x_d)$	Spatial coordinates
\mathcal{M}	Parameter space
p	Number of parameters
$\boldsymbol{\mu} = (\mu_1, \dots, \mu_p)$	Parameter vector
M	Lifting constant
u	Solution of the problem
u_M	Solution of the lifted problem by M
f	Right-hand side of the problem
\mathcal{L}	Parametric differential operator of the problem
R	Reaction coefficient
C	Convection coefficient
D	Diffusion matrix
Pe	Péclet number

Table 24: Notations introduced for the parametric PDE.

Notation	Description
u_θ	Neural network prediction of u
$u_{\theta, M}$	Neural network prediction of u_M
φ	Level-set function used to impose BCs
θ	Trainable parameters of the neural network
θ^*	Optimal parameters
J_r	Residual loss
J_b	Boudary loss
J_{data}	Data loss
J_{sob}	Sobolev loss

Table 25: Notations considered for the neural network.

	Notation	Description
Standard FEM	V_h^0	Finite element approximation space
	u_h	Finite element approximation of u
	h	Characteristic size of the mesh
	\mathcal{I}_h	Lagrange interpolation operator
	k	Polynomial degree of the finite element approximation
Additive enrichment	V_h^+	Finite element approximation space enriched with additive prior
	u_h^+	Finite element approximation of u in V_h^+
	p_h^+	Finite element approximation of $u - u_\theta$ in V_h^0
	C_{gain}^+	Additive gain constant
Multiplicative enrichment	V_h^\times	Finite element approximation space enriched with multiplicative prior
	u_h^\times	Finite element approximation of u in $V_h^\times - M$
	p_h^\times	Finite element approximation of $u_M/u_{\theta,M}$ in $1 + V_h^0$
	$C_{\text{gain},H^1}^\times$	Multiplicative gain constant in H^1 semi-norm
	$C_{\text{gain},L^2}^\times$	Multiplicative gain constant in L^2 norm
	$\tilde{\mathcal{I}}_h$	Modified Lagrange interpolation operator

Table 26: Notations used in the various finite element methods.